A CLEAN SLATE CONTROL FRAMEWORK FOR FUTURE DISTRIBUTION SYSTEMS

A Dissertation

by

YUN ZHANG

Submitted to the Office of Graduate and Professional Studies of
Texas A&M University
in partial fulfillment of the requirements for the degree of

DOCTOR OF PHILOSOPHY

Chair of Committee,	Le Xie
Committee Members,	Prasad Enjeti
	Aniruddha Datta
	Yu Ding
Head of Department,	Miroslav M. Begovic

May 2016

Major Subject: Electrical Engineering

ABSTRACT

This research investigates the microgrid-based solution to future distribution systems with high penetration of distributed energy resources (DERs). A clustered system architecture is envisioned, in which microgrids are formulated as key building blocks of a smart distribution system. Accordingly, the control and operation can be simplified significantly with the system configured as an interconnected of coupling operated microgrids.

By leveraging the highly controllable power electronics (PE) interfaces - voltage source inverters (VSIs), and advanced measurement technology - synchrophasor, we propose a novel interface control strategy, through which desirable power sharing behavior among coupled microgrids can be achieved. Angle droop method is adopted for real power sharing instead of the widely used frequency droop control, which eliminates the need for secondary level frequency control. For reactive power sharing, voltage droop control implemented with integrator is adopted, which provides effective support for voltage dynamics and interaction among interconnected microgrids. Better transient performance can be achieved with the proposed interface control strategy compared with conventional power systems interfaced through synchronous generators (SGs). For the proposed system configuration and interface control strategy, small signal and transient stability problems are investigated. Several criteria are derived, based on which the system stability can be evaluated with computationally efficient algorithms and dynamic security assessed and managed in a timely manner.

With future distribution grids configured as microgrid interconnections, a three level hierarchical control framework is proposed. At the primary level the model

reference control (MRC) is performed for interface parameter online tuning, through which each VSI-interface is controlled to track a designed reference model. At the secondary level, a droop gain management scheme is proposed to adjust the angle and voltage droop gains based on system stability assessment results. At the tertiary level, an AC power flow (ACPF)-based supervisory control strategy is employed to dispatch the nominal setting to each microgrid central controller (MGCC).

DEDICATION

This thesis is dedicated to my husband, Scott, who has provided constant support and encouragement during the challenges of graduate school and life. This work is also dedicated to my parents, Shuwu Zhang and Wenqing Jiang, who have always loved me unconditionally.

ACKNOWLEDGEMENTS

I would like to express my sincere gratitude to my advisor Dr. Le Xie for the guidance and support of my Ph.D study and related research.

I would also like to thank my committee members: Dr. Prasad Enjeti, Dr. Aniruddha Datta and Dr. Yu Ding, for their insightful comments and questions which widened my research scope from various perspectives.

My sincere thanks also goes to our research group members: Fan Zhang, Daehyun Choi, Yingzhong Gu, Omar Urquidez, Chen Yang, Yang Chen, James Carroll, Anupam Thatte, Haiwang Zhong, Sadegh Modarresi, Xiaowen Lai, Meng Wu, Xinbo Geng and Hao Ming.

Last but not least, I would like to thank my family for their constant support and unconditional love.

NOMENCLATURE

AC	Alternating current
ACPF	AC power flow
CP	Connection point
DER	Distributed energy resource
DOE	U.S. department of energy
DSA	Dynamic security assessment
DSO	Distribution system operator
ESS	Energy storage system
GPS	Global positioning system
IED	Intelligent electronic device
LUC	Local unit controller
MGCC	Microgrid central controller
MRAC	Model reference adaptive control
MRC	Model reference control
PCC	Point of common coupling
PE	Power electronic
PMU	Phasor measurement unit
SG	Synchronous generator
SMIB	Single machine infinite bus
SOC	State of charge
TB	Tie branch
VSI	Voltage source inverter
μG	Microgrid

TABLE OF CONTENTS

Page

LIST OF FIGURES

FIGURE Page

LIST OF TABLES

TABLE Page

1. INTRODUCTION*

This research is motivated by the emerging need to design, control and schedule future distribution systems. Today's electric infrastructure is comprised of a complex system of power generation, transmission networks and distribution systems. Electricity is generated by large power plants located near available resource such as hydro and fossil-fuel generation far from load centers. The transmission systems are the vital link between power production and usage responsible for delivering power from remote location of power generation to the commonly populated areas where power is demanded. The distribution systems are responsible for carrying power from the high voltage transmission systems to individual customers [46].

In current industrial practice, distribution systems are mostly passive, less reliable with little intelligence compared with transmission systems [31]. However, technology advancement, environmental concern and economic incentives proliferate the integration of distributed energy resources (DER) [24]. With high penetration level of DER and the related smart grid technologies that in development, future distribution systems will be as active if not more than today's transmission systems. Operating principle used for current distribution grids will not be suitable for the smart and active future distribution systems. Thus novel system architecture and corresponding control and stability assessment frameworks are of urgent need to realized the envisioned smart grid concept.

Smart distribution can be realized through real-time management of all the distributed generation (DG) units integrated; however, timely management of a large

*This section is in part a reprint with permission from Yun Zhang and Le Xie of the material in the paper: "Online Dynamic Security Assessment of Microgrid Interconnections in Smart Distribution Systems," Power Systems, IEEE Transactions on, vol. 30, no. 6, 2015. Copyright 2015 IEEE.

and time variant number of setting points can be an overwhelming task when the DER penetration level becomes high [31]. A promising management strategy is to package DER and associated loads into energy clusters, which are typically referred to as "microgrids". If the system can be configured as an interconnection of microgrids, the task of managing individual DG units with heterogeneous physical nature and dynamical behavior can be simplified. And the number of control points managed by system coordinator will be reduced significantly [31]. In current practice, microgrids are commonly integrated with the external system at a single point of connection, known as the point of common coupling (PCC). The operation status of internal DG units and loads will be managed by the local microgrid central controller, while the PCC voltage profile will be controlled by the distribution system operator for interconnection level management [47].

In this thesis, microgrids are considered as the building blocks for future distribution system with well-designed interaction behavior. Novel interface control strategies are proposed using angle droop method for real power sharing among interconnected microgrids. For a multi-microgrid distribution system with angle droop controlled interfaces, small signal and transient stability criteria are derived allowing for online stability assessment to guarantee system dynamic security. To support high penetration of DERs, a three-level hierarchical control framework is customized for the proposed system configuration. Fig. 1.1 shows the control diagram for the proposed microgrid-based distribution systems.

1.1 The Microgrid Concept

Since its recent introduction, the concept of microgrid has been widely discussed; however, a world-wide "official" definition has not been identified during this research.

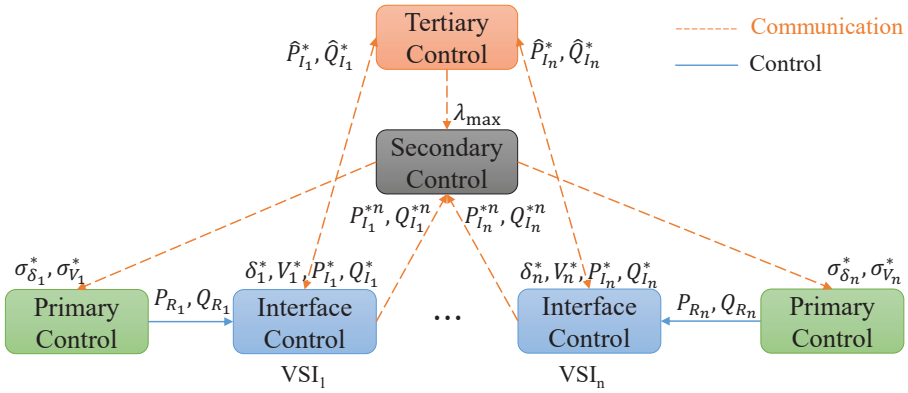

Figure 1.1: Control diagram for microgrid-based distribution systems.

The U.S. Department of Energy (DOE) offered a description of microgrids [43]:

A Microgrid, a local energy network, offers integration of DER with local elastic loads, which can operate in parallel with the grid or in an intentional island mode to provide a customized level of high reliability and resilience to grid disturbances. This advanced, integrated distribution system addresses the need for application in locations with electric supply and/or delivery constraints, in remote sites, and for protection of critical loads and economically sensitive development.

A more succinct definition had been provided later on by the *Microgrid Exchange Group* as follows [4]:

A Microgrid is a group of interconnected loads and distributed energy resources within clearly defined electrical boundaries that acts as a single controllable entity with respect to the grid. A Microgrid can connect and disconnect.

Great efforts had been made to study and construct microgrids. In current practice, microgrids are mostly divided into three categories: 1) remote microgrids, 2) facility microgrids and 3) utility microgrids. The remote microgrids are mostly located in distant areas where the utility grid is inaccessible, and thus do not have

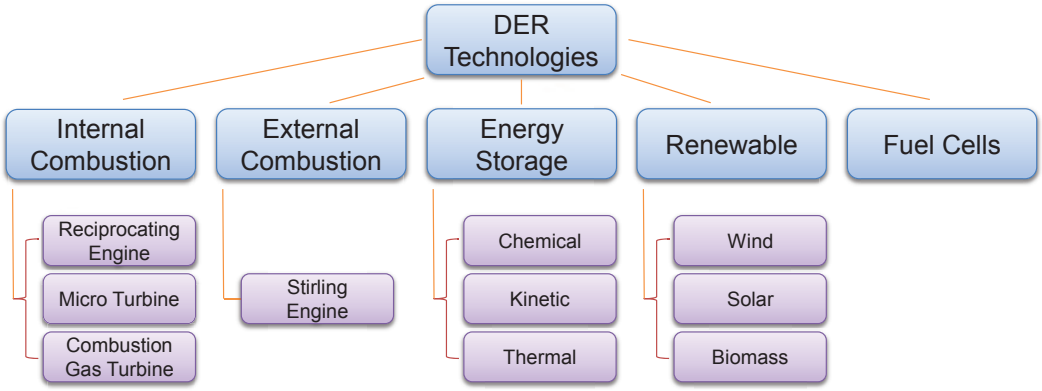

Figure 1.2: Mainstream types of DER technologies.

the grid-connected operation mode. Facility microgrids are typically integrated at the medium voltage level and have little impact on utility grids. Facility microgrids are mainly formulated in North America specifically for industrial or institutional application where technology is matured. Utility microgrids are generally integrated at high voltage level and have massive impact on utility power systems [1].

Different from conventional power systems in which synchronous generators (SG) are the major energy source, electric power is mostly generated though DERs in microgrids. DERs can be considered as small scale power generation units supplying all or a portion of their local loads, and may also be capable of injecting power into the utility grid if local power surplus presents. DER technologies can be largely divided into renewable and nonrenewable depending on their prime movers [46]. Fig. 1.2 shows the mainstream types of DER technologies implemented in current industrial practice [12].

As a collection of technologies with different characteristics, the DER family includes various types of units with heterogeneous profiles. With high level of DER integrated, the net load profiles could be significantly altered, either increasing or reducing peaks [12]. Combining and clustering DERs at the distribution level into

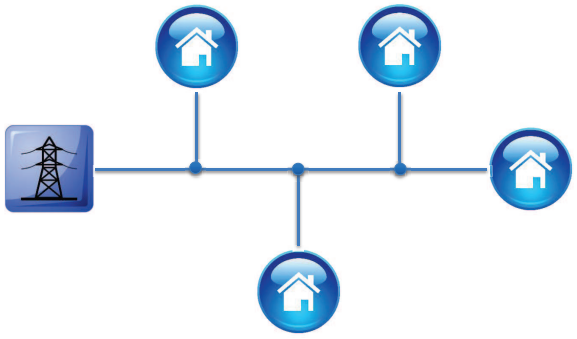

Figure 1.3: Radial distribution system.

the microgrid-based configuration is considered a promising solution to future smart distribution systems [31].

1.2 Architecture of Future Distribution Systems

Two types of distribution system configuration exist in today's practice: radial or network [49]. Arranged like a tree, a radial distribution system involves just one power source for a cluster of clients as shown in Fig. 1.3. It is the least complex and most inexpensive distribution grid to build; however, any failure in the power line will result in a blackout due to the single source configuration. A network distribution system has multiple sources of supply operated in a coupling manner, which provides great opportunities for coupled microgrids application, shown in Fig. 1.4, and adds a huge advantage in terms of reliability [18].

In order to successfully integrate large amount of DERs, many technical challenges must be overcome to guarantee system stability and sustainability and at the meantime ensure that the potential benefits of DERs are fully harnessed [44]. A promising solution is to configure the distribution system as coupling operated microgrids interfaced through power electronic-based interfaces, shown in Fig. 1.4 [60].

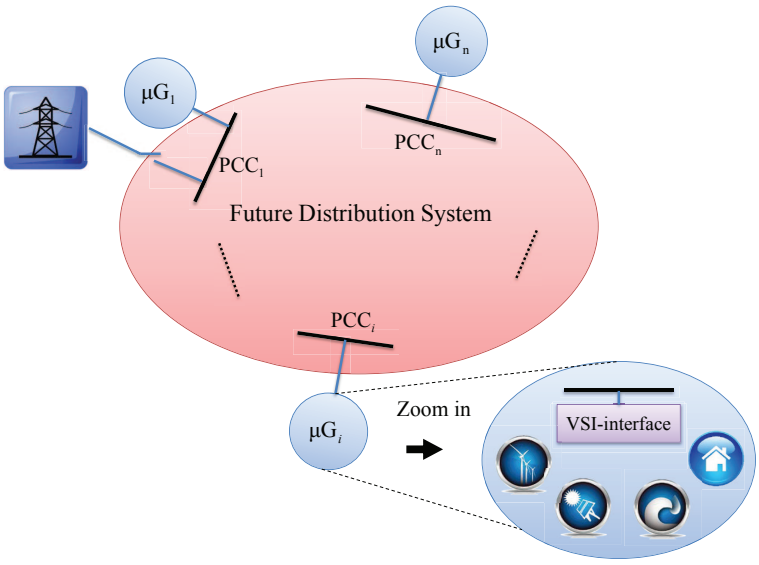

Figure 1.4: Microgrid-based distribution system.

Defined as a energy resource and load cluster, each microgrid packages closely located DER units, energy storage systems and loads at the point of common coupling (PCC) such that the uncontrollable or semi-controllable units (renewable and loads) can be partnered with controllable units (fuel-based sources) and storage. Each power generation and/or consumption unit is controlled by its local unit controller (LUC), and all the LUCs are managed by an intelligent microgrid central controller (MGCC). Then at the upper level, the distribution system operator (DSO) only needs to coordinate each microgrid interface and distributes the task of controlling individual DER units to each microgrid central controller (MGCC) as shown in Fig. 1.5. Such system architecture is similar to the large transmission level multi-machine systems [29], whereas different system interfaces are adopted. Generally, synchronous generators (SGs) are utilized as interfaces for large multi-machine power systems while voltage source inverters (VSI) are widely used as power electronic (PE) interfaces for DER or microgrid considering their advantage in power conversion efficiency and

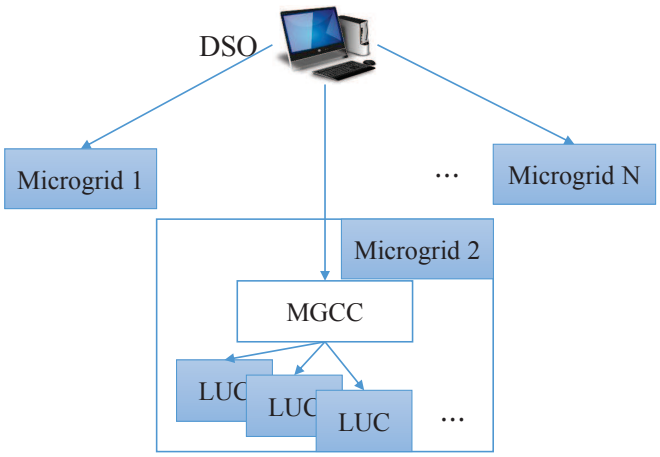

Figure 1.5: Organizational architecture for future distribution systems [62].

their more compact and economical installation compared with current source inverters [27]. With the VSI-based interfaces, the physical inertia on the resource side will be decoupled from the grid side. Thus the interaction behaviors among coupling operated microgrids will be primarily determined by the VSI interface control functions [23].

1.3 Microgrids as Building Blocks of Future Distribution Systems

In current practice, electric power systems are divided into three subsystems, power generation, transmission and distribution systems. Electric power is mostly generated by highly centralized power plants and carried through high voltage transmission network over long distances to consumer communities. At substations, electricity from transmission lines is reduced to lower voltage and supplied to the end customers through distribution systems.

Today's transmission network is by the large reliable and controllable; however, it suffers from cascading failures, low efficiency and poor utilization of resources. Only one third of fuel energy is converted into electric power due to losses in the waste

heat. Further more, around 7% of the electric power generated will be lost in the transmission and distribution lines before delivered to the end customers. Due to the load profile variation, approximately 20% of today's generation capacity is configured just to meet the peak demand existing 5 % of the time. It is expected that these issues aggravated in future grid with high penetration of renewable resources due to their intermittent behavior [31].

On the other hand, today's distribution systems are generally passive, less reliable with little intelligence. Unlike evolutionary step-by-step improvements in transmission systems, revolutionary changes are envisioned providing great opportunity for the "smart grid" concept. In the foreseeable future, large central power plants will continue to serve as bulk power source, while many new customers will be supplied by renewable resources that would today be out of reach of the existing transmission grid. New lines will be built to connect these new resource and customer clusters, and new methods will need to be employed to accommodate their heterogeneous performance characteristic [17].

Bringing electric power sources closer to loads, the microgrid configuration contributes to the voltage profile enhancement, the reduction of transmission and distribution bottlenecks, lower losses, better utilization of waste heat, and postpones investments in large-scale generation and new transmission systems [31]. In the current practice, the power rating of microgrids are still quite small compared with the utility grid. In grid-connected mode, the dynamical impact of a microgrid on the external system is negligible, which validates the single machine infinite bus models commonly used in microgrid dynamical studies. However, when developed into the next level and deployed into large area, microgrids can become building blocks of future distribution systems. Appropriate control and management strategy needs to be in place so that a microgrid can be presented to the macro grid as a well-behaved

single controllable entity.

1.4 Challenges for Systematic Control of Coupling Operated Microgrids

The control and operation problems of *individual* microgrid have been studied extensively, e.g. topology formulation, power management strategy, islanding and resynchronizing operation, etc. [31], [48], [55]. For stability studies, small signal stability of microgrids was investigated in [41], which proposes an adaptive droop controller ensuring relative stability at different loading conditions. In [22], a stability assessment approach is proposed for parallel-connected inverters to examine the system (microgrid) stability in a decentralized manner. However, it still remains an open area of research for the coupling operation of microgrids at the interconnection level. High penetration of intermittent energy resources could have significant effect on the dynamic behaviors of microgrids. Excessive interaction of microgrids could result in power swings and losing synchronized coupling even if all microgrids are individually stabilized. A systematic stability analysis could provide key insights for the distribution system operator to effectively assess system-wide dynamic security of microgrid interconnections.

In large scale system theory, a well-established method for stability analysis of interconnected systems is to utilize properties of individual subsystems in conjunction with the interconnection structure to obtain sufficient conditions for asymptotic stability in the large [42], [2]. Numerous stability analysis algorithms and results for interconnected systems had been tailored and applied to conventional power systems, e.g. [45], [5]. However, several fundamental and unique features differ interconnected microgrids from conventional power systems: 1) energy resources are commonly integrated through power electronic (PE) converters decoupling their physical inertia from the grid; 2) the (external) behavior of microgrids will be primarily determined

by the control scheme of their interfaces; 3) microgrids are generally integrated at the distribution level, where lines cannot be considered lossless; 4) commonly, intelligent electronic devices (IEDs) with synchro-phasor capability are equipped at the PCC to realize seamless transition between grid-connected and islanded modes; 5) modeling and control framework capable of handling meshed networks might be desirable with an eye to their potential for loss reduction and better support of DER integration [10]. Clearly these unique features advocate a fresh control framework customized for the coupling operation of microgrids in future smart distribution systems.

1.5 Main Contributions

In this thesis, the microgrid concept is taken to the next level. Microgrids are considered as the fundamental building blocks of the future smart distribution systems. Presented to the macro grid as single controllable entities, the control and management task for the distribution system operator can be greatly simplified.

To achieve desirable interaction behavior, a novel interface control strategy is proposed, in which angle droop method is adopted for real power sharing control, while voltage droop method, the version implemented with integrator, is adopted for reactive power sharing.

For the microgrid-based system architecture with the proposed interface control strategy, small-signal and transient stability problems are studied. For small-signal stability, a coordinated criterion is derived based on a sufficient and necessary condition obtained with Lyapunov theorem, while a distributed criterion is derived based on a sufficient condition obtained with dissipative system theory and Lyapunov direct method. For transient stability, a sufficient condition is derived based on the linear matrix inequality (LMI) version of the Kalman-Yakubovich-Popov (KYP) conditions. With these stability criteria, system-wide stability can be assessed in a real

time manner, which is highly desirable for systems with large amount of highly intermittent resources integrated.

For systems with fast changing operating condition, a three-level hierarchical control framework is proposed to guarantee system performance, through which conservativeness can be reduced significantly in the design of microgrid power sharing characteristics.

2. DISSERTATION OUTLINE

The rest of this dissertation is organized as follows. Section 3 introduces the proposed microgrid interface control strategies. For real power sharing, angle droop method is compared with the widely used frequency droop control with their pros and cons discussed in detail. For reactive power sharing, voltage droop method implemented with integrator is introduced. With the interface control strategy determined, dynamical model the microgrid module is presented. This section also describes a virtual interfacing scheme for the internal integration VSIs when no physical interface unit is deployed at the microgrid point of common coupling.

Section 4 presents the stability assessment of multi-microgrid systems. Small-signal and transient stability criteria are derived, based on which system-wide stability can be assessed in a real time manner.

Section 5 presents the proposed hierarchical control framework for future distribution systems to guarantee system-wide stability, in which three control levels are defined. A model reference control (MRC)-based scheme is adopted for online droop gaining tuning at the primary level, through which the interface inverter of each microgrid is controlled to track a designed reference model. At the secondary level, an interactive droop management scheme is proposed to manage the reference model droop gains based on derived system stability criteria. At the tertiary level, an AC power flow (ACPF)-based supervisory control strategy is utilized to 1) dispatch the nominal setting to each microgrid central controller (MGCC) for the primary level reference tracking, and 2) broadcast an interaction coefficient to each MGCC so that the droop gains can be managed to guarantee system-wide stability. This section also presents the management scheme for microgrids interfaced through multiple VSIs.

Section 6 presents the numerical studies of some example test systems. A single machine infinite bus system is formulated to demonstrate the proposed interface control strategy and virtual interfacing scheme. Small-signal stability is evaluated for a 5-microgrid study system formulated based on IEEE 123-node test feeder. Transient stability is evaluated for this 5-microgrid but with different tie-branch parameters. Also with this 5-microgrid system, numerical examples are formulated to demonstrate the feasibility of the proposed hierarchical control framework.

Section 7 summaries the main contributions of this thesis and presents the topic to be studied in future work.

3. INTERFACE CONTROL STRATEGY FOR MICROGRID INTERACTION

3.1 Power Sharing and Interaction among Coupled Microgrids

To manage interaction and power sharing among interconnected units, different strategies exist in current practice of distributed generation integration.

- Master/Slave Strategy. This strategy is widely used for managing DER units inside a microgrid, in which internal DER units delivers voltage, current or power injection profile according to the command of a master unit. The master unit will be dedicated to power balancing in islanded mode or microgrid interface control in grid-connected mode [59].

- Droop-based Control Strategy. Droop method does not require critical communication among electrically coupled units. Each unit adjusts its output setting according to designed droop characteristics. This strategy is suitable for interaction and power sharing control in multi-microgrid distribution systems. Power sharing without communication among microgrids is the most desirable option as the distribution network can be complex and spanning over a large geographic area [40].

3.2 Angle Droop Control for Real Power Sharing

Concerning the interfacing of microgrids to the distribution system, it is important that proper power sharing achieved among coupling operated microgrids. Droop-based methods are highly desirable due to their minimal communication requirement as the distribution systems can be complex and span over large areas [38]. Motivated by SG operation principle, frequency droop method is mostly adopted using local frequency signals (real power balance indicator) as feedback to control

respective interface output. Depending on the stiffness of the power-frequency curve, the steady state frequency will change with the time varying power production and consumption mismatch. It is widely known that in order to achieve stable operation, the alternating current (AC) frequency must be held within tight tolerance bounds. Such high requirement of frequency regulation limits the allowable range of frequency droop gain, which in turn, may lead to chattering during frequent load change or renewable resource fluctuation [40]. If all the microgrids are interfaced through VSIs as shown in Fig. 1.4, the output voltage angle of each interface can be set arbitrarily as long as a synchronized angle reference is available [60]. Thus drooping the VSI voltage angle instead of frequency can be a better option for power sharing considering its advantage in transient performance and control flexibility [60], [38], [39].

In current practice of microgrid interface control, algorithms mimicking SG swing equations are commonly used to craft synthetic inertia in case that the system frequency is at risk of running into unacceptable level following resource and/or load disturbances [63]. Such algorithms are basically frequency droop methods utilizing the frequency deviation signal as power balance indicator due to the nature of SG swing equations. Nevertheless, several factors limit their application for future distribution systems: 1) in order to achieve zero steady-state frequency deviation, the synchronization frequency ω_{sync} need to be accessed by each interface VSI, which is unfortunately not locally available. Thus the conventional droop methods do not allow for plug-and-play realization despite their distributed implementation [53]; 2) the conflict between frequency regulation requirement and the sensitivity of indicating power imbalance [37]. The frequency regulation constraint limits the allowable range of the droop gains.

In the case of VSI-interfaced microgrids, the output angle can be changed instan-

taneously, and thus drooping the angle is a better way for real power sharing. Better system transient performance could be expected with the angle droop method. For the angle droop control methods signals from the global positioning system (GPS) are required for angle referencing, which can be available from deployed intelligent electronic devices (IEDs) with phasor measurement units (PMUs) embedded [38].

In current practice, the frequency droop methods dominate in real power sharing control among coupled microgrids [15], [40], [41]. Such methods manage the frequency setting according to the following relationship.

$$\omega^{ref} = \omega^* + \sigma_\omega(P_I^* - P_I), \tag{3.1}$$

where P_I^* and P_I are the nominal and actual real power injection of the microgrid. σ_ω is the frequency droop gain.

With (3.1), the $P - \delta$ subsystem dynamics can be represented as follows.

$$\Delta\dot{\delta} = \Delta\omega = -\sigma_\omega \Delta P_I, \tag{3.2}$$

where $\Delta P_I = P_I - P_I^*$ represents the real power imbalance. $\Delta\omega = \omega^{ref} - \omega^*$.

If synchrophasor measurement is available, then angle damping can be added so that

$$\Delta\dot{\delta} = -D_\delta \Delta\delta - \sigma_\omega \Delta P_I, \tag{3.3}$$

where $\Delta\delta = \delta - \delta^*$, D_δ is the angle damping coefficient.

With simple manipulation, (3.3) can be rewritten as follows.

$$\tau_\delta\dot{\delta} + \delta - \delta^* = \sigma_\delta(P_I^* - P_I), \tag{3.4}$$

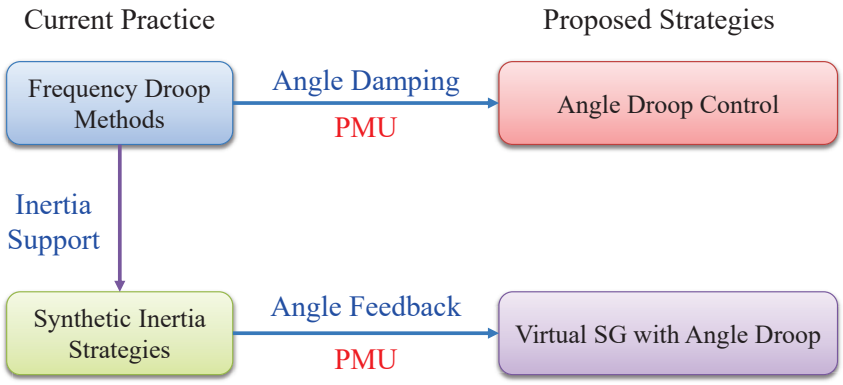

Figure 3.1: Current practice and proposed interface control strategies.

where $\tau_\delta = \frac{1}{D_\delta}$ is the time constants for angle tracking. $\sigma_\delta = \frac{\sigma_\omega}{D_\delta}$ is the angle droop gain.

From previous discussion, the following advantages come with the angle droop control strategy: 1) secondary level frequency regulation can be avoided; 2) asymptotical stability can be achieved even when no infinite bus presents in the system model; 3) for a multi-microgrid interconnection, small signal stability can be evaluated in a distributed manner, which provides insightful guidance for droop gain design of each microgrid interface.

3.3 Angle Feedback Control for Interfaces Providing Inertia Support

For large power rating applications that have significant impact on the transmission system, there is concern that the inertia-less power electronic interfaces may result in noticeable decrease of overall system inertia so that following large power plant trips, the system frequency will be at risk of falling below the acceptable limit before frequency control can respond to mitigate the situation [63]. Synthetic inertia strategies emulating synchronous generator (SG) behaviors have been proposed to address this issue [14], [9], [63], [8]. The eletro-static energy stored in the DC link

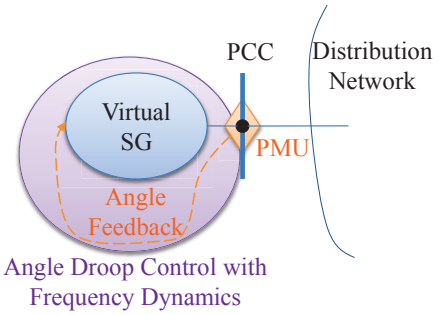

Figure 3.2: Diagram of inertia emulating interfaces with angle feedback control.

capacitors can be managed to emulate the kinetic energy transition behavior of SGs [63]. Correspondingly, the $P-\delta$ subsystem dynamics of inertia emulating interfaces can be represented as follows.

$$\begin{aligned} \Delta\dot{\delta} &= \Delta\omega, \\ J\Delta\dot{\omega} &= -D\Delta\omega - \sigma_\omega \Delta P_I, \end{aligned} \tag{3.5}$$

where J is the virtual inertia constant determined by the SG emulation strategy.

Here we propose an angle feedback control scheme for the SG emulating interfaces so that the angle droop characteristic follows with the aforementioned advantages. The relationship among between the state of the art and the proposed strategies are given in Fig. 3.1.

Assuming synchrophasor measurement is available at the microgrid PCC, angle feedback control can be utilized to craft the interface SG emulation behavior with angle droop characteristics, diagram given in Fig. 3.2.

With angle feed back control adopted for a SG-emulating interface i, the small

signal model of its $P-\delta$ subsystem can be represented as follows [60], [20].

$$\begin{aligned} \Delta\dot{\delta}_i &= \Delta\omega_i, \\ J_i\Delta\dot{\omega}_i &= -D_i\Delta\omega_i + \Delta P_{C_i} - \Delta P_{I_i}, \\ \tau_{C_i}\Delta\dot{P_{C_i}} &= -\Delta P_{C_i} - K_{C_i}\Delta\delta_i \end{aligned} \tag{3.6}$$

where ΔP_{C_i} is the angle feedback control variable, τ_{C_i} is the controller response time constant, K_{C_i} is the angle feedback gain.

3.4 Voltage Droop Control for Reactive Power Sharing

For reactive power sharing, voltage droop method is widely used employing the following control function.

$$V - V^* = \sigma_V(Q_I^* - Q_I), \tag{3.7}$$

where Q_I^*, Q_I are the nominal and actual reactive power injection. σ_V is the voltage droop gain.

It is clear that if a microgrid injects a non-zero amount of reactive power Q_I, its voltage will deviate from its reference V^* according to the droop characteristic defined in (3.7). To avoid sudden change in interface voltage, an integral channel can be added yielding the first-order voltage droop controller [54]. Implemented with integrator, we have the following voltage control function representing the Q-V subsystem dynamics.

$$\tau_V\dot{V} + V - V^* = \sigma_V(Q_I^* - Q_I), \tag{3.8}$$

where τ_V is the time constants for voltage tracking.

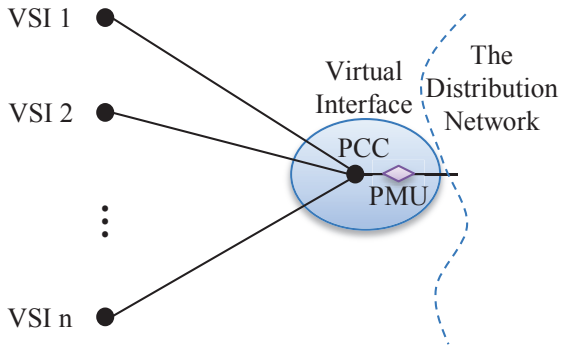

Figure 3.3: DER integration VSIs and microgrid virtual interface.

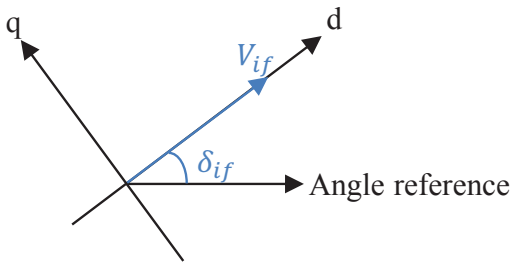

Figure 3.4: The d-q axis alignment.

3.5 Distributed Control of Multiple VSIs for Virtual Interfacing

If no interface VSI is deployed at the microgrid PCC, virtual interfacing can be realized by managing the integration VSI of each internal DER unit. Fig. 3.3 shows the diagram of a microgrid with n DER units integrated. The PCC voltage is not directly controlled by an interface VSI although synchrophasor measurement is available.

By definition each microgrid acts as a single controllable entity for the interconnection level analysis, of which the dynamics is determined by the control strategy of a virtual interface. With angle and voltage droop methods adopted for real and

reactive power interaction, respectively, the PCC voltage phase angle and magnitude of each microgrid need to be generated as follows according to (3.4), (3.8).

$$\begin{aligned} \delta_{if} &= \delta^* + \frac{\sigma_\delta}{\tau_\delta s + 1}(P_I^* - P_I), \\ V_{if} &= V^* + \frac{\sigma_V}{\tau_V s + 1}(Q_I^* - Q_I). \end{aligned} \tag{3.9}$$

$V_{if}\angle\delta_{if}$ can not be generated directly since there is no interface VSI deployed at the microgrid PCC; however, it can be generated indirectly by managing the integration VSI of each DER unit in a distributed manner.

Using the d-q equivalent circuit of the balanced three phase PCC voltage, the d axis can be aligned with $V_{if}\angle\delta_{if}$ as shown in Fig. 3.4. Then the d and q axis current injection from the PCC to the network can be calculated as

$$I_d = \frac{P_I}{V_{if}},\ I_q = -\frac{Q_I}{V_{if}}. \tag{3.10}$$

For the kth DER integration VSI, $k = 1 \dots m$, let its d and q axis output current be

$$I_{d_k} = c_{d_k} I_d,\ I_{q_k} = c_{q_k} I_q, \tag{3.11}$$

where c_{d_k} and c_{q_k} are the participation factors of VSI k respectively for d and q axis current injection to the network, which are assigned by the MGCC satisfying

$$\sum_{i=1}^{m} c_{d_k} = 1,\ \sum_{i=1}^{m} c_{q_k} = 1. \tag{3.12}$$

Note the line impedance from VSI k to the PCC as

$$z_k = R_k + jX_k, \tag{3.13}$$

we have,

$$V_{d_k} + jV_{q_k} - V_{if} = (R_k + jX_k)(I_{d_k} + jI_{q_k}). \tag{3.14}$$

Then the d and q axis output voltage of VSI k can be calculated as

$$\begin{aligned} V_{d_k} &= V_{if} + R_k I_{d_k} - X_k I_{q_k}, \\ V_{q_k} &= R_k I_{q_k} + X_k I_{d_k}. \end{aligned} \tag{3.15}$$

The corresponding voltage setting for the DER integration VSIs can be obtained as

$$\begin{aligned} V_k^{ref} &= |V_{d_k} + jV_{q_k}|, \\ \delta_k^{ref} &= \delta_{if} + \tan^{-1}(\frac{V_{q_k}}{V_{d_k}}), \end{aligned} \tag{3.16}$$

where $k = 1 \ldots n$.

The above procedure can be simplified if the current injection of each VSI is determined by its electrical distance to the microgrid PCC through controlling all VSIs with the same voltage reference. All the equal-potential VSI nodes can be represented as one equivalent node connected to the microgrid PCC through a line with impedance

$$z_{eq} = \frac{1}{\sum_{k=1}^{n} \frac{1}{z_k}} = R_{eq} + jX_{eq}. \tag{3.17}$$

Then the d and q axis voltage for each VSI will be

$$\begin{aligned} V_d &= V_{if} + R_{eq} I_d - X_{eq} I_q, \\ V_q &= R_{eq} I_q + X_{eq} I_d. \end{aligned} \tag{3.18}$$

And the voltage reference setting for each VSI will be

$$\begin{aligned} V^{ref} &= |V_d + jV_q|, \\ \delta^{ref} &= \delta_{if} + \tan^{-1}(\frac{V_q}{V_d}). \end{aligned} \tag{3.19}$$

4. STABILITY ASSESSMENT FOR MICROGRID-BASED DISTRIBUTION SYSTEMS*

In order to successfully integrate large amount of DERs, many technical challenges must be overcome to guarantee system stability and sustainability and at the meantime ensure that the potential benefits of DERs are fully harnessed [44]. Stability assessment is considered a fundamental and important problem in power system design and operation [51].

4.1 Representation of Microgrid Modules for System-wide Stability Analysis

In the proposed system configuration, each microgrid is connected to the system at the point of common coupling (PCC) through a VSI interface with synchrophasor measurement capability. Angle and voltage droop methods are utilized for autonomous real and reactive power sharing among interconnected microgrids. At the PCC of interface $i \in \{1, \ldots, n\}$, we specify the angle and voltage droop control law by combining (3.4) and (3.8).

$$\begin{aligned} \tau_{\delta_i}\dot{\delta}_i + \delta_i - \delta_i^* &= \sigma_{\delta_i}(P_{I_i}^* - P_{I_i}), \\ \tau_{V_i}\dot{V}_i + V_i - V_i^* &= \sigma_{V_i}(Q_{I_i}^* - Q_{I_i}), \end{aligned} \tag{4.1}$$

where δ_i, V_i are the PCC voltage angle and magnitude. $P_{I_i}^*$, $Q_{I_i}^*$ are the nominal real and reactive power injections. P_{I_i}, Q_{I_i} are the actual real and reactive power injections. τ_{δ_i}, τ_{V_i} are the angle and voltage tracking time constants. σ_{δ_i}, σ_{V_i} are the angle and voltage droop gains which represent the sensitivity of indicating real and

*This section is in part a reprint with permission from Yun Zhang and Le Xie of the material in the paper: "Online Dynamic Security Assessment of Microgrid Interconnections in Smart Distribution Systems," Power Systems, IEEE Transactions on, vol. 30, no. 6, 2015. Copyright 2015 IEEE.

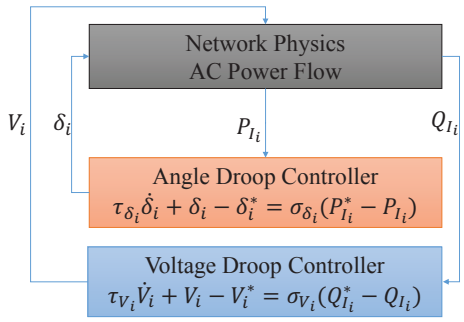

Figure 4.1: Feedback loop for the proposed droop controller.

reactive power imbalance, respectively.

Then in the n-microgrid interconnected system, dynamical behavior of each interface is determined by the control law given in (4.1), and constrained by the network physics in an instantaneously coupling manner, as shown in Fig. 4.1. For the ith microgrid in the system, it is well known that its real and reactive power injection P_{I_i}, Q_{I_i} are related with the interface states V_i, δ_i through the power flow equations governed by Kirchoff's law. P_{I_i} and Q_{I_i} are not locally determined but the result of system interaction, which can be considered as the feedback from the network. The key idea of the proposed microgrid interface control strategy is to define the real and reactive power sharing characteristics according to the angle and voltage droop control function. The interface states δ_i and V_i are determined by the network feedback measurement P_{I_i}, Q_{I_i}, together with the reference setting $P_{I_i}^*, \delta_i^*$, $Q_{I_i}^*, V_i^*$ dispatched by the DSO.

The nominal real and reactive power injections $P_{I_i}^*$, $Q_{I_i}^*$ are dispatched by the DSO solving an AC power flow problem and remain constant during a dispatch interval, e.g. 15 minutes. The actual real and reactive power injections are determined by the

following power angle relationship.

$$\begin{aligned} P_{I_i} &= V_i^2 G_{ii} + \sum_{k=1,\ k\neq i}^{n} V_i V_k Y_{ik} sin(\delta_{ik} + \pi/2 - \theta_{ik}), \\ Q_{I_i} &= -V_i^2 B_{ii} + \sum_{k=1,\ k\neq i}^{n} V_i V_k Y_{ik} sin(\delta_{ik} - \theta_{ik}), \end{aligned} \tag{4.2}$$

where G_{ii} is the self-conductance of the ith microgrid, and Y_{ik}, θ_{ik} are, respectively, the modulus and phase angle of the transfer admittance between the ith and the kth microgrids.

For a n-microgrid distribution system, the equilibrium states of interest are the solutions of (4.1) and (4.2) with $\dot{\delta}_i = 0, \dot{V}_i = 0$, and $P_{I_i} = P^*_{I_i}, Q_{I_i} = Q^*_{I_i}$, $i = 1 \dots n$. The nominal power injections $P^*_{I_i}, Q^*_{I_i}, i = 1 \dots n$ satisfy the AC power flow equations given in (4.3).

$$\begin{aligned} P^*_{I_i} &= V_i^{*2} G_{ii} + \sum_{k=1,\ k\neq i}^{n} V_i^* V_k^* Y_{ik} sin(\delta^*_{ik} + \pi/2 - \theta_{ik}), \\ Q^*_{I_i} &= -V_i^{*2} B_{ii} + \sum_{k=1,\ k\neq i}^{n} V_i^* V_k^* Y_{ik} sin(\delta^*_{ik} - \theta_{ik}). \end{aligned} \tag{4.3}$$

4.2 Small-signal Stability of Coupled Microgrids without Inertia Support

For a n-microgrid distribution system, the local stability properties of the equilibrium solution δ^*_i, V^*_i, $P^*_{I_i}$, $Q^*_{I_i}$, $i = 1 \dots n$, can be derived from linearizing (4.1), (4.2) and (4.3) around the equilibrium solution. The corresponding small signal (SS) model of the n-microgrid system can be formulated as in (4.4).

$$\begin{aligned} \dot{x} &= A^s x + B^s u, \\ u &= Jx, \end{aligned} \tag{4.4}$$

where

$$x = [x_1^T \ \dots \ x_n^T]^T, \ u = [u_1^T \ \dots \ u_n^T]^T,$$

in which $x_i = [\Delta\delta_i, \Delta V_i]^T$, $u_i = [\Delta P_{I_i}, \Delta Q_{I_i}]^T$, and

$$A^s = diag(A_i^s), \ B^s = diag(B_i^s), i = 1 \dots n,$$

in which

$$A_i^s = \begin{bmatrix} -\frac{1}{\tau_{\delta_i}} & \\ & -\frac{1}{\tau_{V_i}} \end{bmatrix}, \ B_i^s = \begin{bmatrix} -\frac{\sigma_{\delta_i}}{\tau_{\delta_i}} & \\ & -\frac{\sigma_{V_i}}{\tau_{V_i}} \end{bmatrix}.$$

J is the extended power flow Jacobian matrix formatted as

$$J = \begin{bmatrix} \frac{\partial u_1}{\partial x_1} & \cdots & \frac{\partial u_1}{\partial x_n} \\ \vdots & \ddots & \vdots \\ \frac{\partial u_n}{\partial x_1} & \cdots & \frac{\partial u_n}{\partial x_n} \end{bmatrix}. \tag{4.5}$$

Since the small signal (SS) model (4.4) is linear and time invariant, it suffices to evaluate the eigenvalues of the matrix $A_{cl}^s = A^s + B^s J$. Small signal stability of the system equilibrium can be concluded if all the eigenvalues of A_{cl}^s have negative real parts. Small signal stability assessed through eigenvalue analysis only suggests that the system solutions tend to the equilibrium of interest for initial conditions sufficiently close to it. However, it is important not only to establish such local stability properties of the equilibrium solution, but also to study the transient stability properties when the system experiences large disturbances. Similar with conventional transient analysis, we will focus on the synchronization stability of interconnected systems, which falls into the category of short-term angle stability problems.

4.2.1 Coordinated Stability Criterion

If all the eigenvalues of A^s have negative real parts, the system is asymptotically stable. With high penetration level of DERs, a large number of interconnected microgrids may need to be managed in real time to realize smart distribution. Computing eigenvalues of a large-scale system matrix is not a trivial task, thus the corresponding assessment could be challenging for on-line applications.

Here instead, we consider the well-known Lyapunov theorem [30]: the system (4.17) is stable if and only if there exists a positive-definite matrix P such that

$$A^{sT}P + PA^s < 0, \tag{4.6}$$

which can be formulated as a convex optimization problem involving LMIs [56]. Actually, this is a convex feasibility problem which can be solved by interior-point algorithms [6].

Accordingly, the above coordinated stability criterion can be stated as follows.

Criterion 1 [60]: the multi-microgrid system (4.17) is asymptotically stable if and only if the LMIs problem (4.7) is feasible.

$$\begin{aligned} A^{sT}P + PA^s < 0, \\ P > 0. \end{aligned} \tag{4.7}$$

4.2.2 Distributed Stability Criterion

For the coupling operation of a large number of microgrids, it would be desirable to perform on-line assessment of system-wide stability in a distributed manner. As a natural generalization of Lyapunov theory for open systems, the dissipative system theory is very useful for analyzing interconnected systems [56], [57]. Accordingly the

following procedures can be performed: 1) given that the interfacing control strategy ensures module local stability, dissipative dynamic equivalents (singular-perturbed model) are obtained for all microgrid modules; 2) based on the module equivalents, their storage functions can be constructed as Lyapunov function candidates; 3) each module agent assess system stability with a distributed criterion derived based on an upper bound of the module interaction strength; 4) system-wide stability may be concluded by collecting the assessment results from module agents.

For a general minimal finite dimensional linear system (FDLS) represented by state space matrices A, B, C, D, the dissipativeness can be evaluated from the LMIs in (4.8).

$$\begin{aligned} \begin{bmatrix} A^TQ + QA & QB - C^T \\ B^TQ - C & -D - D^T \end{bmatrix} \leq 0, \\ Q = Q^T \geq 0. \end{aligned} \tag{4.8}$$

According to Theorem 3 of [57], the minimal FDLS is dissipative with respect to the supply rate $w = \langle u, y \rangle$ if and only if (4.8) has a solution. And with solution Q, the function $\frac{1}{2}\langle x, Qx \rangle$ defines a quadratic storage function. Here $\langle x, y \rangle$ stands for the inner product of vector x and y.

For the ith microgrid, (3.4) and (3.8) can be rewritten into the state space form (4.9).

$$\begin{aligned} \dot{x}_i &= A_i x_i + B_i u_i, \\ y_i &= C_i x_i, \end{aligned} \tag{4.9}$$

where $x_i = [\Delta\delta_i, \Delta V_i]^T$, $u_i = [-\Delta P_{I_i}, -\Delta Q_{I_i}]^T$, $C_i = I$ so that $y_i = x_i$. And

$$A_i = \begin{bmatrix} -\frac{1}{\tau_{\delta_i}} & \\ & -\frac{1}{\tau_{V_i}} \end{bmatrix}, \; B_i = \begin{bmatrix} \frac{\sigma_{\delta_i}}{\tau_{\delta_i}} & \\ & \frac{\sigma_{V_i}}{\tau_{V_i}} \end{bmatrix}.$$

Since the model (4.9) is strictly proper with $D_i = D_i^T = 0$, the LMIs in (4.8) reduces to (4.10) with the unique solution $Q_i = B_i^{-1}$.

$$\begin{aligned} A_i^T Q_i + Q_i A_i \leq 0, \; Q_i B_i = C_i^T = I, \\ Q_i = Q_i^T > 0. \end{aligned} \tag{4.10}$$

Hence, module i is dissipative with respect to $\langle u_i, y_i \rangle$ if the interface control strategy generates positive angle droop gain and voltage droop gain, since

$$\begin{aligned} Q_i = Q_i^T = B_i^{-1} &= \begin{bmatrix} \frac{\tau_{\delta_i}}{\sigma_{\delta_i}} & \\ & \frac{\tau_{V_i}}{\sigma_{V_i}} \end{bmatrix} > 0, \\ A_i^T Q_i + Q_i A_i &= 2 \begin{bmatrix} -\frac{1}{\tau_{\delta_i}} & \\ & -\frac{1}{\tau_{V_i}} \end{bmatrix} \begin{bmatrix} \frac{\tau_{\delta_i}}{\sigma_{\delta_i}} & \\ & \frac{\tau_{V_i}}{\sigma_{V_i}} \end{bmatrix} \\ &= 2 \begin{bmatrix} -\frac{1}{\sigma_{\delta_i}} & \\ & -\frac{1}{\sigma_{V_i}} \end{bmatrix} < 0. \end{aligned}$$

Rearrange the n-module system modeled (4.4) into the following state space form.

$$\begin{aligned} \dot{x} &= Ax + Bu, \\ u &= -Hx, \end{aligned} \tag{4.11}$$

where

$$x = [x_1^T \ \dots \ x_n^T]^T, \ u = [u_1^T \ \dots \ u_n^T]^T,$$

in which $x_i = [\Delta\delta_i, \Delta V_i]^T$, $u_i = [-\Delta P_{I_i}, -\Delta Q_{I_i}]^T$, and $A = diag(A_i), \ B = diag(B_i)$. H is the same as the extended Jacobian matrix J defined in (4.5).

Formulate the system-wide storage matrix as $Q = B^{-1} = diag(Q_i)$. Clearly with all modules dissipative, Q is positive definite. Consider the time derivative of the storage function $S(x) = \frac{1}{2}\langle x, Qx\rangle$, we have

$$\begin{aligned} \dot{S(x)} &= \frac{1}{2}(\dot{x}^T Q x + x^T Q \dot{x}) \\ &= \frac{1}{2}[x^T (A - BH)^T Q x + x^T Q (A - BH) x] \\ &= x^T (AQ - \frac{H^T + H}{2}) x. \end{aligned} \tag{4.12}$$

Obviously, $S(x)$ is a Lyapunov function if $M^{c1} = AQ - \frac{H^T+H}{2}$ is negative definite.

Notice that $F = -\frac{H^T+H}{2}$ is a Hermitian matrix, $F^T = F$ and all of its entries are real. According to Theorem 8.1.4 in [30], the Rayleigh quotient for a Hermitian matrix is bounded by its eigenvalues:

$$\lambda_{min} = min \ R_F(x), \ \lambda_{max} = max \ R_F(x), \tag{4.13}$$

where $R_F(x) \triangleq \frac{\langle Fx,x\rangle}{\langle x,x\rangle}$, λ_{min} and λ_{max} correspond to the smallest and largest eigenvalue of F. Here λ_{max} is defined as the interaction coefficient representing a upper bound of coupling strength of modules for a specific system operation condition.

Then following (4.12), we have

$$\begin{aligned} \dot{S(x)} &= x^T(AQ - \frac{H^T + H}{2})x \\ &= x^T AQx + x^T Fx \\ &\leq x^T AQx + \lambda_{max} x^T x \\ &= \sum_1^N x_i^T (A_i Q_i + \lambda_{max} I) x_i, \end{aligned}$$

Thus if $M_i^c, i = 1 \ldots N$ are all negative definite, the interconnected system is asymptotically stable.

Accordingly, the distributed stability criterion can be stated as follows.

Criterion 2 [60]: If a) the interconnected system (4.17) have all modules exhibit positive inertia and damping coefficients, and b) the assessment matrices $M_i^c = A_i Q_i + \lambda_{max} I, i = 1 \ldots N$ are all negative definite, then the system is asymptotically stable.

This is a distributed criterion in the sense that it only requires each microgrid module to check their internal stability property. The assessment can be performed by each agent checking its angle feedback gain K_i and voltage droop gain σ_{V_i} since

$$A_i Q_i + \lambda_{max} I = \begin{bmatrix} -\frac{1}{\sigma_{\delta_i}} + \lambda_{max} & \\ & -\frac{1}{\sigma_{V_i}} + \lambda_{max} \end{bmatrix}. \tag{4.14}$$

The only piece of information need to be broadcast by the system coordinator is the interaction coefficient λ_{max} defined in (4.13). It can be obtained through calculating the extended Jacobian matrix defined in (4.5) based on real time operation condition.

4.3 Small-signal Stability of Coupled Microgrids with Inertia Support

As discussed in Section 3.3, synthetic inertia can be added to the interface control function if inertia support is required by the transmission network, to which the microgrid-based distribution system is connected.

4.3.1 System Modeling and Order Reduction

With inertia support, each microgrid can be represented as in (3.6) and (3.8), and thus the model of a n-microgrid system can be formulated in the following state space form.

$$\begin{bmatrix} \Delta\dot{\delta} \\ \Delta\dot{V} \\ \varepsilon\Delta\dot{\omega} \\ \varepsilon\Delta\dot{P}_C \end{bmatrix} = \begin{bmatrix} O & O & I & O \\ O & A_V & O & O \\ O & O & A_\omega & F_\omega \\ F_f & O & O & A_f \end{bmatrix} \begin{bmatrix} \Delta\delta \\ \Delta V \\ \Delta\omega \\ \Delta P_C \end{bmatrix} + \begin{bmatrix} O & O \\ O & B_V \\ B_\omega & O \\ O & O \end{bmatrix} \begin{bmatrix} \Delta P_I \\ \Delta Q_I \end{bmatrix}, \quad (4.15)$$

where $\Delta\delta = [\Delta\delta_1 \dots \Delta\delta_n]^T$, $\Delta V = [\Delta V_1 \dots \Delta V_n]^T$, $\Delta\omega = [\Delta\omega_1 \dots \Delta\omega_n]^T$, $\Delta P_I = [\Delta P_{I_1} \dots \Delta P_{I_n}]^T$, $\Delta Q_I = [\Delta Q_{I_1} \dots \Delta Q_{I_n}]^T$. Here the perturbation parameter $\varepsilon = 1$. O represents the $n \times n$ zero matrix, I represents the $n \times n$ identity matrix. And $A_V = -diag(\frac{1}{\tau_{V_i}})$, $B_V = -diag(\frac{\sigma_{V_i}}{\tau_{V_i}})$, $A_\omega = -diag(\frac{D_i}{J_i})$, $B_\omega = -diag(\frac{1}{J_i})$, $F_\omega = diag(\frac{1}{J_i})$, $A_f = -diag(\frac{1}{\tau_{C_i}})$, $F_f = -diag(\frac{K_{C_i}}{\tau_{C_i}})$, , $i = 1 \dots n$.

In (4.15) the real and reactive power injections P_I, Q_I are related with δ, V by the power flow equations [3]. Thus through linearizion ΔP_I, ΔQ_I can be related with $\Delta\delta$, ΔV as follows.

$$\begin{bmatrix} \Delta P_I \\ \Delta Q_I \end{bmatrix} = \bar{H} \begin{bmatrix} \Delta\delta \\ \Delta V \end{bmatrix} = \begin{bmatrix} \bar{H}_{11} & \bar{H}_{12} \\ \bar{H}_{21} & \bar{H}_{22} \end{bmatrix} \begin{bmatrix} \Delta\delta \\ \Delta V \end{bmatrix}, \quad (4.16)$$

in which $\bar{H}$ can be obtained by rearranging the extended Jacobian matrix J defined in (4.5).

For differential systems having dynamics evolving in multiple time scales, it is not practical in most cases to handle all dynamics in a single model. The so called "time scale decomposition" technique is commonly used to solve such problems [19]. Assuming that the fast modes converge quickly to the algebraic equations as $\varepsilon = 0$, the system (4.15) and (4.16) reduces to

$$\begin{bmatrix} \Delta\dot{\delta} \\ \Delta\dot{V} \end{bmatrix} = \begin{bmatrix} A_\delta & O \\ O & A_V \end{bmatrix} \begin{bmatrix} \Delta\delta \\ \Delta V \end{bmatrix} + \begin{bmatrix} B_\delta & O \\ O & B_V \end{bmatrix} \bar{H} \begin{bmatrix} \Delta\delta \\ \Delta V \end{bmatrix}, \tag{4.17}$$

where $A_\delta = A_\omega^{-1} F_\omega A_f^{-1} F_f = -diag(\frac{K_{C_i}}{D_i})$, $B_\delta = -A_\omega^{-1} B_\omega = -diag(\frac{1}{D_i})$.

Clearly, the order-reduced system model (4.17) can be rearranged into the form of (4.4) with simple manipulation.

4.3.2 Stability of the Order-reduced System

The stability of system (4.17) can be evaluated by checking the eigenvalues of the state matrix

$$A_S = A^R + B^R \bar{H} \tag{4.18}$$

where $A^R = blkdiag(A_\delta, A_V)$, $B^R = blkdiag(B_\delta, B_V)$.

It is clear that the order-reduced system model (4.17) cab be rearranged into the same form of the system model without inertia support (4.11). Thus the coordinated and distributed criteria derived in Section 4.2 can also be applied to evaluate the small-signal stability of the order-reduced system (4.17).

4.3.3 Stability of the Original System

Assume by design the order-reduced system (4.17) is stable, i.e. A_S defined in (4.18) is a Hurwitz matrix with all eigenvalues having negative real parts. The stability bound problem of the singular perturbed system modeled in (4.15) and (4.16) can be formulated to find the maximal singular perturbation parameter ε^*, such that for all $0 \leq \varepsilon < \varepsilon^*$ system (4.15), (4.16) is stable given the stability of the order reduced system (4.17) [7].

The linear time-invariant (LTI) singular perturbed system (4.15) can be rearranged into the following partitioned form.

$$\begin{bmatrix} \dot{x_1} \\ \dot{x_2} \end{bmatrix} = \begin{bmatrix} A_{11} & A_{12} \\ \frac{A_{21}}{\varepsilon} & \frac{A_{22}}{\varepsilon} \end{bmatrix} \begin{bmatrix} x_1 \\ x_2 \end{bmatrix} \triangleq A(\varepsilon)x, \tag{4.19}$$

where $A_{11} = \begin{bmatrix} O & O \\ B_V\bar{H}_{21} & A_V + B_V\bar{H}_{22} \end{bmatrix}$, $A_{21} = \begin{bmatrix} F_\omega + B_\omega\bar{H}_{11} & B_\omega\bar{H}_{12} \end{bmatrix}$,

$A_{12} = \begin{bmatrix} I \\ O \end{bmatrix}$, $A_{22} = A_\omega$.

The stability bound problem is to find the maximal positive parameter ε^* such that $A(\varepsilon)$ is stable for all $0 < \varepsilon < \varepsilon^*$. For this ε-bound problem [28] gives an important result as stated in the following lemma.

Lemma 1 (Kokotovic et al. [28]): If both $A_0 = A_{11} - A_{12}A_{22}^{-1}A_{21}$ and A_{22} are Hurwitz stable matrices, then there exists an ε^* such that for all $\varepsilon \in (0, \varepsilon^*)$, the full-order system (4.19) is stable.

According to Lemma 1, there must exist an infinitely small $\varepsilon = 0^+ > 0$ such that system (4.19) is stable, i.e. all eigenvalues of $A(\varepsilon)|_{\varepsilon=0^+}$ have negative real parts. Thus when the perturbation parameter ε sweep from $\varepsilon = 0^+$ to $\varepsilon > \varepsilon^*$, either 1) a real

eigenvalue of $A(\varepsilon)$ enters the right half plane via the origin, or 2) a pair of conjugate complex eigenvalues passes the imaginary axis to the right half plane if $\varepsilon^* \neq \infty$. For the special case $\varepsilon = \varepsilon^*$, some eigenvalues of $A(\varepsilon)$ will lie on the imaginary axis [7].

With the following Lemma, this stability bound problem can be converted to a equivalent non-singularity analysis problem.

Lemma 2 (Lancaster et al. [30]): Let the eigenvalues of matrices $A \in \mathscr{R}^{m\times m}$ and $B \in \mathscr{R}^{n\times n}$ be $\lambda_1, \ldots \lambda_m$ and $\mu_1 \ldots \mu_n$, respectively. Then the eigenvalues of their Kronecker product $A \bigotimes B$ are the mn products of the form $\lambda_j \mu_k$, $1 \leq j \leq m$ and $1 \leq k \leq n$. And the eigenvalues of their Kronecker sum, defined as $A \bigoplus B \triangleq A \bigotimes I_{n\times n} + I_{m\times m} \bigotimes B$, are of the mn sums of the form $\lambda_j + \mu_k$.

According to Lemma 2, if all eigenvalues of matrix $A(\varepsilon)$ lie in the open left half plane, all the eigenvalues of $A(\varepsilon) \bigoplus A(\varepsilon)$ lie in the open left half plane as well, which means that $A(\varepsilon) \bigoplus A(\varepsilon)$ is nonsingular. Thus $A(\varepsilon)$ Hurwitz stable $\Leftrightarrow$ $A(\varepsilon) \bigoplus A(\varepsilon)$ nonsingular. Then the stability bound problem of system (4.19) can be solved with the following Theorem.

Theorem 1 (Liu et al. [34]): The stability bound ε^* of system (4.19) is:

$$\varepsilon^* = min\{\alpha_i : \alpha_i \in \lambda_R^+(N, -M)\}, \tag{4.20}$$

where $\lambda_R^+(N, -M)$ is the set of finite positive real generalized eigenvalues of the matrix pair N and $-M$, i.e. $\lambda_R^+ = \{\alpha \in \mathscr{R}^+ : det(N + \alpha M) = 0\}$ [7]. And

$$\begin{aligned} M &\triangleq \begin{bmatrix} A_{11} & A_{12} \\ O_{n\times 2n} & O_{n\times n} \end{bmatrix} \bigoplus \begin{bmatrix} A_{11} & A_{12} \\ O_{n\times 2n} & O_{n\times n} \end{bmatrix}, \\ N &\triangleq \begin{bmatrix} O_{2n\times 2n} & O_{2n\times n} \\ A_{21} & A_{22} \end{bmatrix} \bigoplus \begin{bmatrix} O_{2n\times 2n} & O_{2n\times n} \\ A_{21} & A_{22} \end{bmatrix}. \end{aligned} \tag{4.21}$$

If no finite positive real eigenvalues exists for $(N, -M)$, define $\varepsilon^* \triangleq +\infty$.

In our study system the perturbation parameter $\varepsilon = 1$, thus according to Theorem 1, the following criterion is proposed for stability assessment of a SG-interfaced n-microgrid system.

Criterion 3: if the order-reduced system (4.17) is stable, i.e. the state matrix in (4.18) is Hurwitz stable, and the perturbation parameter bound obtained with Theorem 1 is larger than 1, i.e. $\varepsilon^* > 1$, then the original system modeled in (4.19) or (4.15) is also stable.

4.4 Transient Stability Assessment

Small signal stability only suggests that the system solutions tend to the equilibrium of interest for initial conditions sufficiently close to it. However, it is important not only to establish the local stability properties of the equilibrium solution, but also to study the transient stability properties when the system experiences large disturbances.

It had been shown that conventional power system interfaced through SGs are generally not asymptotically stable in the large [58]. There are often multiple equilibrium solutions due to two essential factors: 1) the second order SG swing equation; 2) the sinusoidal power angle relationship. For the proposed multi-microgrid distributed system with angle droop controlled VSI interfaces, it will be shown that asymptotically stable in the large may be achieved with conservative droop gain design. On the other hand if voltage phase angle of all interfaces can be contained in a limited range, conservativeness in droop gain design can be significantly reduced.

In practical situations, the voltage regulation behavior is generally much slower than the transient phenomena which are of interest in transient stability studies [58]. If for each microgrid interface, τ_{V_i} is much larger than τ_{δ_i} by design, the PCC voltage

can then be assumed constant during the transient period, i.e. $V_i = V_i^*$. And the transient stability problem can be significantly simplified.

Note $z_i = \delta_i - \delta_i^*$, $i = 1 \dots n$, and let m_i be the number of branches connected to the ith microgrid. Then from (4.1), (4.2) and (4.3) we have,

$$\begin{aligned} \tau_{\delta_i} \dot{z}_i + z_i &= -\sigma_{\delta_i} \sum_{j=1}^{m_i} e_j \phi_j(y_j), \\ \phi_j(y_j) &= sin(y_j + y_j^0) - sin y_j^0, \end{aligned} \tag{4.22}$$

where $e_j = V_i^* V_k^* Y_{ik}$, $y_j = z_i - z_k = \delta_{ik} - \delta_{ik}^*$, and $y_j^0 = \delta_{ik}^* + \pi/2 - \theta_{ik}$.
Formulate the incidence matrix H and the connectivity matrix C such that the n-microgrid system with states $z = [z_1 \dots z_n]^T$ and output $y = [y_1 \dots y_n]^T$ can be represented as follows.

$$\begin{aligned} \dot{z} &= Az + B\phi(y), \\ y &= Cz, \end{aligned} \tag{4.23}$$

where $A = diag(-1/\tau_{\delta_i})$, $D = diag(-\sigma_{\delta_i}/\tau_{\delta_i})$, $i = 1 \dots n$. $E = diag(e_j)$, $j = 1 \dots m$. $B = DHE$. The system nonlinearities $\phi(y) = [\phi_1(y_1) \dots \phi_m(y_m)]^T$. It should be noted that here $m = \sum_{i=1}^{n} m_i$ equals to twice the total number of system branches.

The n-microgrid system represented by (4.23) is a multi-variable Lur'e system with time invariant sector-bounded memoryless nonlinearities. From (4.22) we see that the functions ϕ_j, $j = 1 \dots m$ satisfy the $[-1, 1]$ sector conditions

$$-y_j^2 \leq y_j \phi_j(y_j) \leq y_j^2, \ j = 1 \dots m, \tag{4.24}$$

for all $y_i \in \mathbb{R}$.

In order to prove stability of the system (4.23) with nonlinearity sector conditions

given in (4.24), a loop transformation procedure can be performed [6]. Define

$$\bar{\phi}_j(y_j) = \frac{1}{\beta_j - \alpha_j}(\phi_j(y_j) - \alpha_j y_j), \tag{4.25}$$

where the sector lower bound $\alpha_j = -1$ and the sector upper bound $\beta_j = 1$ for all $j = 1 \dots m$.

Obviously $0 \leq y_j\bar{\phi}_j(y_j) \leq y_j^2$ for all $y_j \in \mathbb{R}$. Let $\Lambda = diag(\alpha_j)$ and $\Gamma = diag(\beta_j - \alpha_j)$, so that $\bar{\phi}(y) = \Gamma^{-1}(\phi(y) - \Lambda y)$. Substitute $\phi(y) = \Gamma\bar{\phi}(y) + \Lambda y$ into (4.23), we have

$$\begin{aligned} \dot{z} &= \bar{A}z + \bar{B}\bar{\phi}(y), \\ y &= \bar{C}z, \end{aligned} \tag{4.26}$$

where $\bar{A} = (A + B\Lambda C)$, $\bar{B} = B\Gamma$ and $\bar{C} = C$.

Now the nonlinearities are contained within $[0, 1]$ sectors

$$0 \leq y_j\bar{\phi}_j(y_j) \leq y_j^2, \ j = 1 \dots m, \tag{4.27}$$

or, equivalently,

$$\bar{\phi}_j(y_j)(\bar{\phi}_j(y_j) - y_j\bar{\phi}_j(y_j)) \leq 0, \ j = 1 \dots m, \tag{4.28}$$

for all $y_i \in \mathbb{R}$.

To prove stability of the n-microgrid system represented by (4.26), consider the Lyapunov function of the form

$$V(z) = z^T P z + 2\sum_{j=1}^{m} \lambda_j \int_0^{\bar{C}_j z} \bar{\phi}_j(y_j)\ dy_j, \tag{4.29}$$

where $\bar{C}_j$ denotes the ith row of $\bar{C}$.

According to Lyapunov theorem, seek P and λ_j, $j = 1 \dots m$, such that

$$\frac{dV(z)}{dt} < 0, \tag{4.30}$$

for all nonzero z satisfying (4.26) and (4.27).

The $\mathcal{S}$-procedure [6] can be utilized to derive sufficient condition for (4.30):

The LMI in $P > 0$, $\Lambda = diag(\lambda_j) \leq 0$ and $T = diag(\tau_j)$, $j = 1 \dots m$,

$$\begin{bmatrix} \bar{A}^T P + P\bar{A} & P\bar{B} + \bar{A}^T \bar{C}^T \Lambda + \bar{C}^T T \\ \bar{B}^T P + \Lambda \bar{C} \bar{A} + T\bar{C} & \Lambda \bar{C} \bar{B} + \bar{B}^T \bar{C}^T \Lambda - 2T \end{bmatrix} < 0 \tag{4.31}$$

holds [61].

4.5 Stability Assessment Framework

In this section, a stability assessment framework, shown in Fig. 4.2, is proposed for future distribution systems, which can be implemented online to guarantee system-wide operation stability. In Section 4.2, coordinated and distributed criteria are derived, based on which the system small-signal stability can be evaluated online in a timely manner. In Section 4.4, sufficient condition for system transient stability is derived for based on Lyapunov direct method. The Lyapunov function proving transient stability is obtained by solving the LMIs formulated based on the multi-variable Popov criterion. As a general numerical method, the proposed small-signal and transient stability assessment criteria are well suited for automatic computation and can be integrated into the droop management procedure at the secondary control level to guarantee system transient stability.

The stability condition in (4.31) is actually the LMI version of Kalman-Yakubovich-Popov conditions corresponding to the multi-variable Popov criterion [16]. The sys-

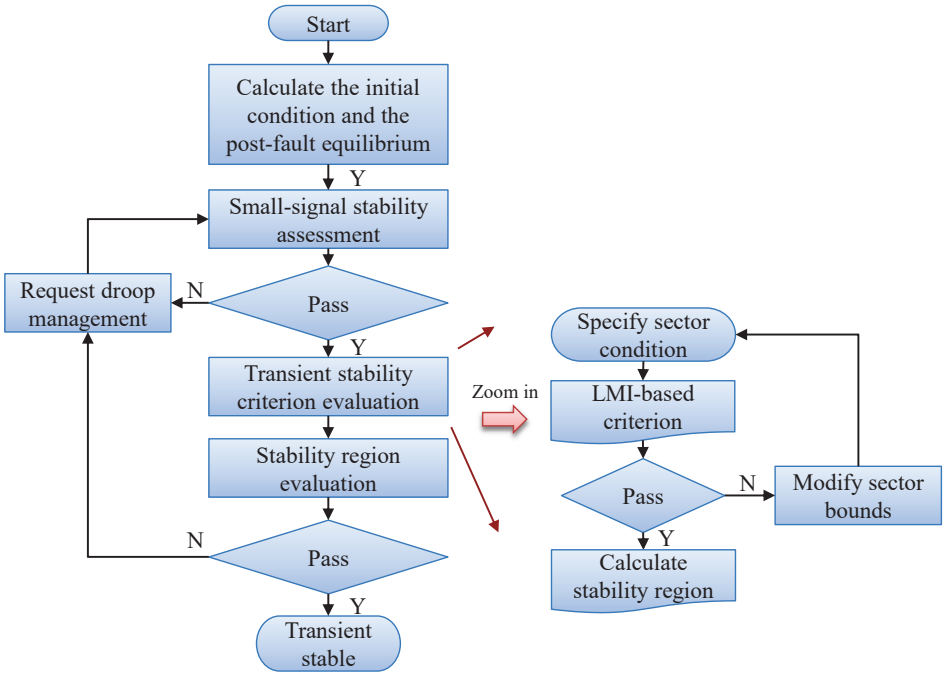

Figure 4.2: Stability assessment framework.

tem will be asymptotically stable (a.s.) in the large if the LMIs given in (4.31) are feasible. However, this global stability criterion will require the angle droop gains σ_{δ_i}, $i = 1 \dots n$ to be sufficiently small, which may result in over-conservative design of interface control with limited droop-based power sharing capability. Such conservativeness can be significantly reduced with the following procedure:

Step 1: consider the sectors $\phi_j(y_j) \in [-1, 1]$, $j = 1 \dots m$;

Step 2: transform the sectors to $[0, 1]$ according to (4.26);

Step 3: solve the LMIs formulated in (4.31);

Step 4: if (4.31) is feasible the system (4.23) is a.s. in the large, otherwise go to Step 5;

Step 5: take the upper half of the sectors and perform Step 2;

Step 6: perform Step 3;

Step 7: if the LMIs in (4.31) are feasible, regional stability can be concluded and goto Step 6, otherwise goto Step 5;

Step 6: calculate guaranteed stability region according to the sector condition specified in Step 5;

Step 7: if the initial condition z_0 falls into the stability region the system (4.23) will be transient stable and $z_0 \to 0$ at steady state, otherwise droop management will be requested for smaller angle droop gains.

The above procedure is integrated into the stability assessment framework, as shown in Fig.4.2 [61].

4.6 Application in Distribution System Black Start

As an ancillary service, black start is procured for the restoration of the power system in the event of a complete or partial blackout. Generating units with self start capability are contracted, e.g. on an annual basis, to start up the predefined system restoration and load recovery process. To be capable of providing black start service, on-site diesel or gas turbine generators are commonly deployed to power the auxiliary systems of a large generating unit, which can be started by batteries or other form of energy storage devices. Once in service, the large generating unit can be used to energize part of the local network and provide supplies for other stations within its service area [50]. In current practice, system restoration is performed by managing the contracted black start units in a top-down manner, beginning with the start-up of black start units and ending with the connection of loads. And the restoration service is generally carried out manually according to predefined guidelines and procedures [50], [36].

Black start of future distribution systems is an innovative and promising aspect for fully harnessing the benefits from the potentialities of microgrid-based configura-

tion. By definition, microgrids are capable of running in the islanded mode servicing their critical loads [23]. And also, generally with some form of energy storage systems embedded microgrids possess self-start capability, and thus can be natural candidates for black start resources when developed to the commensurate power scale. A corresponding bottom-up black start strategy can be utilized to assist system restoration after a complete or partial blackout is experienced by the envisioned future distribution systems configured as coupling operated microgrids.

It would be inefficient in both the technical and economical sense if all conventional power plants were obliged to provide a black start service [50]; however, configured as multi-microgrid systems, future distribution networks could manage restoration from all microgrids simultaneously.

4.6.1 Microgrid Black Start for Local Restoration

The black start of each microgrid involves a sequence of control actions defined through predefined rules and criteria to be checked during the local restoration stage. In order to provide the performance required of a black start service, the following technical capabilities are required for a microgrid [36]:

- Autonomous local power supply feeding local control systems and to launch local generation.
- Bidirectional communication between the microgrid central controller (MGCC) and the local controller (LC) of each distributed generation (DG) unit.
- Updated information about local load status, generation profile and the availability of DGs to black start.
- Automatic load management after system collapse, e.g. disconnection of selected (non-critical) demand blocks.

- Islanding from the distribution network before the black start procedure.

During microgrid local restoration, a set of electrical problems had been identified in [36] for the black start procedure:

- Building the internal low voltage (LV) network, including the distribution transformer energization.
- Connecting DGs.
- Regulating voltage magnitude and frequency.
- Connection controllable demand blocks.

And a sequence of actions defined to restore microgrid service as follows [35].

- Partitioning the microgrid around each DG with black start capability allowing it to feed its own critical loads.
- Building the internal LV network.
- Synchronizing the black start DG islands.
- Connecting controllable loads.
- Restoring service of uncontrollable load and DG units.

4.6.2 Microgrid Resynchronization for System Restoration

After local service is restored for some microgrids and the medium voltage (MV) network re-energized and available for their coupling operation, stability conditions

need to be verified before operating grid connection switches for microgrid resynchronization. Then those microgrids can be resynchronized and clustered into multi-microgrid islands and finally merged together as a whole synchronized interconnection.

During the microgrid resynchronization procedure, it is assumed that 1) each microgrid is interfaced through a VSI of which the PCC voltage angle and magnitude can be directly managed; 2) synchrophasor measurement (PMU) is available at each microgrid PCC. Then the following procedure can be performed for module (or group of modules) synchronization.

Step 1: calculate the post synchronization operation point o^{K+1} with the estimated power injection of each microgrid $\hat{P_{I_i}}, \hat{Q_{I_i}}$, $i = 1 \dots n$.

Step 2: evaluate system transient stability from the initial condition $o^K = (1\angle 0^\circ \dots 1\angle 0^\circ)$ to the post synchronization operation point o^{K+1} according to the assessment framework shown in Fig. 4.2.

Step 3: if the transient stability criterion (4.31) discussed in Section 4.5 is passed, dispatch the reference setting to each microgrid according to o^{K+1} and close the inter-microgrid tie-breakers. Break the loop as the system is synchronized successfully.

Step 4: if the transient stability criterion (4.31) is not passed, let $\hat{P'_{I_i}} = 0.5\hat{P_{I_i}}, \hat{Q'_{I_i}} = 0.5\hat{Q_{I_i}}$, $i = 1 \dots n$, and calculate the corresponding post synchronization operation point $o^{K+1'}$.

Step 5: go to Step 2.

5. HIERARCHICAL CONTROL FRAMEWORK FOR FUTURE DISTRIBUTION SYTEMS*

The control and operation problems of *individual* microgrid have been studied extensively, e.g. topology formulation, power management strategy, islanding and resynchronizing operation, etc. [31], [48], [55]. For stability studies, small signal stability of microgrids was investigated in [41], which proposes an adaptive droop controller ensuring relative stability at different loading conditions. In [22], system (microgrid) stability is investigated for parallel-connected inverters. However, it still remains an open area of research for the coupling operation of microgrids at the interconnection level. High penetration of intermittent energy resources could have significant effect on the dynamic behaviors of microgrids. Excessive interaction of microgrids could result in power swings and losing synchronism even if all microgrids are individually stabilized.

Assuming voltage source inverters (VSIs) are readily deployed as interfaces, a hierarchical control framework is proposed for future distribution systems to guarantee system-wide stability, in which three control levels are defined as shown in Fig. 5.1. A model reference control (MRC)-based scheme is adopted for online droop gaining tuning at the primary level, through which the interface inverter of each microgrid is controlled to track a designed reference model. At the secondary level, an interactive droop management scheme is proposed to manage the reference model droop gains based on derived system stability criteria. At the tertiary level, an AC power flow (ACPF)-based supervisory control strategy is utilized to 1) dispatch the nominal

*This section is in part a reprint with permission from Yun Zhang and Le Xie of the material in the paper: "Interactive Control of Coupled Microgrids for Guaranteed System-wide Small Signal Stability," Smart Grid, IEEE Transactions on, to appear, 2016. Copyright 2016 IEEE.

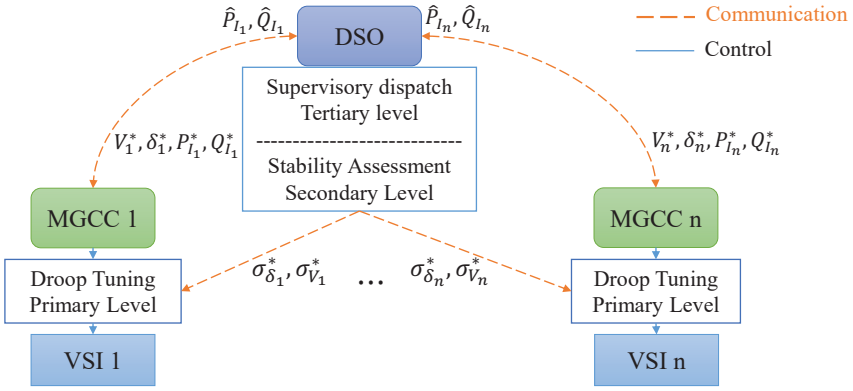

Figure 5.1: The interactive control framework for future distribution systems.

setting to each microgrid central controller (MGCC) for the primary level reference tracking, and 2) broadcast an interaction coefficient to each MGCC so that the droop gains can be managed to guarantee system-wide stability [62].

5.1 Primary Level Control for Droop Gain Tuning

Assuming voltage source inverters (VSIs) are readily deployed as interfaces, the envisioned smart distribution system can be configured as interconnected microgrids. At the primary level, the interface VSIs can be controlled to 1) shape the microgrid external behavior with desirable dynamical response characteristic, 2) track the reference droop characteristics designed based on steady-state performance standards and system-wide stability criterion.

Considering microgrids as aggregated units interfaced through VSIs, the PCC voltage of each microgrid could be shaped through the interface control scheme implemented by the MGCC [60], [23], [33]. For effective load sharing among VSI-interfaced units, droop-based methods are widely used to achieve a communication free control realization [44]. Originated from the power balancing principle of synchronous generators in large power systems, frequency deviation from nominal value is commonly

used as the indicator of local real power mismatch, i.e. an imbalance between the input mechanical power and output electric real power will cause a change in local frequency. Similarly, voltage magnitude deviation indicates local reactive power mismatch [60]. Emulating the behaviors of synchronous generators, frequency-droop methods are commonly used for real power sharing [25], [23], [13], [41], [15]; however, the acceptable range of frequency deviation is tightly constrained by the regulation requirement. Using frequency droop for real power sharing may cause the so-called "chattering" phenomenon with high penetration of inertia-less units interfaced by VSIs [37]. Actually, both the dynamical behavior and droop characteristics of an interface VSI can be artificially crafted [44] by its control function implemented. With synchrophasor measurement available for each interface VSI, angle droop methods can be used for real power sharing. Instead of frequency deviation, the difference between the interface VSI voltage phase angle and a synchronized reference is employed to indicate local real power mismatch. With angle droop methods, better dynamic performance can be expected [37], [32].

In our previous work [60], an interface control strategy is proposed using angle-droop (P-δ) method for real power sharing and voltage droop (Q-V) for reactive power sharing. Corresponding stability criteria are derived to evaluate system-wide small signal stability. Here taking a step further, we propose a MRC-based scheme for the primary level control to track a reference model designed at the secondary level based on a distributed system-wide stability criterion. As an angle droop based method, signals from the global positioning system (GPS) are required for angle referencing, but no communication is necessary among the interface VSIs at the primary level [37].

When external behaviors of a VSI-interfaced microgrid is studied at the interconnection level, only the interface control function is modeled with the fast switching

transients and high frequency harmonics neglected as a common practice [44]. The objective of the interface control is to track the nominal setting of the PCC voltage, i.e. $V_t\angle\delta_t$ tracking its reference setting $V_t^{ref}\angle\delta_t^{ref}$. Taking advantage of fast responding power electronic switches, the switching frequency can be designed much higher than the PCC voltage fundamental frequency in consideration of power quality. Thus the phasor representation $V_t\angle\delta_t$ is validated to represent the averaged VSI behavior without compromising modeling accuracy.

In current practice of droop-based interface control, the droop gains are commonly pre-designed at fixed and very conservative values to guarantee system stability for all the possible operation points [23], [13]. Consequently, the ability of autonomous power sharing among microgrids will be significantly limited. Such control design approach does not require online tuning, whereas the operation optimality will be significantly sacrificed since the droop gains need to be constrained by the worst case scenario of all. Especially for a system with large penetration level of renewable energy a wide range of operating conditions need to be considered, which deteriorates autonomous power sharing capability. Here we propose a MRC-based scheme at the primary control level for droop gain online tuning of each microgrid interface so that the real time system stability and regulation requirement satisfied with respect to a specific operation point dispatched by the DSO.

With the proposed interface control scheme implemented, dynamics of each microgrid can be represented as follows.

$$\begin{aligned} \tau_\delta\dot{\delta} + \delta - \delta^* &= \sigma_\delta(P_G + P_R - P_L - P_I), \\ \tau_V\dot{V} + V - V^* &= \sigma_V(Q_G + Q_R - Q_L - Q_I), \end{aligned} \tag{5.1}$$

where $\tau_\delta = \frac{1}{D_\delta}$ is the time constants for angle tracking. $\sigma_\delta = \frac{\sigma_\omega}{D_\delta}$ is the angle droop

gain. Q_G is the total reactive power generated in the microgrid. Q_R corresponds to the total reactive power for regulation, which can be controlled for model reference tracking. Q_L is the total reactive power consumption. Q_I is the reactive power injection. τ_V is the time constants for voltage tracking. σ_V is the voltage droop gain.

With the plant model (5.1), the objective is to choose an appropriate control law such that all signals in the closed-loop plant are bounded and the states δ, V track the desired values δ_r, V_r of the reference model given by

$$\begin{aligned} \tau_{\delta_r}\dot{\delta}_r + \delta_r - \delta^* &= \sigma_{\delta_r}(P_I^* - P_I), \\ \tau_{V_r}\dot{V}_r + V_r - V^* &= \sigma_{V_r}(Q_I^* - Q_I), \end{aligned} \tag{5.2}$$

where P_I^*, Q_I^* are nominal real and reactive power injection. τ_{δ_r}, τ_{V_r} are the designed time constants for tracking voltage angle and magnitude, respectively, which range from several to tens of seconds for smoothing out fast disturbance. σ_{δ_r},σ_{V_r} are the P-δ and Q-V droop characteristics determined by the secondary level control scheme.

In order to track the reference model (5.2), we propose the following control law

$$\begin{aligned} P_R &= -k_P^*(\delta - \delta^*) + l_P^*(P_I^* - P_I) - P_G + P_L + P_I, \\ Q_R &= -k_Q^*(V - V^*) + l_Q^*(Q_I^* - Q_I) - Q_G + Q_L + Q_I, \end{aligned} \tag{5.3}$$

where k_P^*, l_P^*, k_Q^*, l_Q^* are control parameters to be calculated.

The close-loop dynamical model can be obtained by combining (5.1) and (5.3).

$$\begin{aligned} \frac{\tau_\delta}{1+\sigma_\delta k_P^*}\dot{\delta} + \delta - \delta^* &= \frac{\sigma_\delta l_P^*}{1+\sigma_\delta k_P^*}(P_I^* - P_I), \\ \frac{\tau_V}{1+\sigma_V k_Q^*}\dot{V} + V - V^* &= \frac{\sigma_V l_Q^*}{1+\sigma_V k_Q^*}(Q_I^* - Q_I). \end{aligned} \tag{5.4}$$

If the plant model parameters were known, by matching the transfer function of

(5.4) with that of (5.2), the control parameters can be calculated as follows.

$$k_P^* = \frac{\tau_\delta - \tau_{\delta_r}}{\tau_{\delta_r}\sigma_\delta}, l_P^* = \frac{\tau_\delta \sigma_{\delta_r}}{\tau_{\delta_r}\sigma_\delta}, k_Q^* = \frac{\tau_V - \tau_{V_r}}{\tau_{V_r}\sigma_V}, l_Q^* = \frac{\tau_V \sigma_{V_r}}{\tau_{V_r}\sigma_V}. \tag{5.5}$$

The above transfer function matching approach guarantees that the close-loop plant states converge to the reference model exponentially fast for any bounded signal [21]

$$r_i(t) = [P_I^*(t) - P_I(t), Q_I^*(t) - Q_I(t)]^T. \tag{5.6}$$

Depending on how the VSI control is implemented, the up to date plant model parameters might be unknown to the MGCC. Then an adaptive law can be implemented with on-line estimates of the plant model parameters. And the corresponding direct or indirect model reference adaptive control (MRAC) schemes can be utilized for the aforementioned control objective [21].

The key idea of the proposed MRC-based scheme is to reshape the interface characteristics according to a designed reference model through managing available regulation power. We will show in the following that how the reference model can be determined at the secondary level to guarantee system-wide stability.

5.2 Secondary Level Droop Management for Guaranteed System-wide Stability

In conventional power systems, the secondary level control is commonly implemented to eliminate the frequency deviation from its nominal value introduced by the $P - \omega$ droop control. With the proposed angle droop control method, the frequency deviation approaches zero at the steady state. Thus the frequency restoration process is not necessary. Instead, a droop management scheme is proposed here to guarantee system-wide stability at the secondary level, shown in Fig. 5.2. Implemented by MGCCs, droop gains satisfying the small-signal and/or transient stability

can be calculated based on the stability assessment result. Accordingly, the desirable $P-\delta$, $Q-V$ droop gains can be designed for reference model to be tracked at the primary level. Then the stability reserve for each microgrid can be controlled for the primary level MRC tracking.

In traditional power systems, regulating reserves participate in the finest scale of balancing during normal conditions. Regulating reserves are responsible for correcting the imbalance from the total load or generation that differs from the forecast condition. Provided by the governor response, regulating reserves modify the droop gain of each synchronous generator participating in primary level control. Since normal imbalances usually do not trigger frequency response, the governor control parameters are designed based on system regulation requirement and stability constraint through contingency analysis [11]. Reserves are commonly not used for system stabilization due to the response speed limit of conventional units. However in future distribution systems with high penetration of VSI interfaced units (or clusters), stability reserves might be applicable taking advantage of the fast responsive power electronic interfaces. Other than the regulating and following reserves commonly configured in conventional large power systems, here we propose to deploy stability reserves to ensure real time system-wide stability. Energy battery storage systems can be good candidates for stability reserves since 1) they can be deployed at the DC link of each microgrid PCC and controlled by the fast responding interface VSI; 2) they can provide both upward and downward reserves for automatic stabilization.

In order to perform the online droop gain tuning scheme defined at the primary level, we propose to configure stabilizing resource for each microgrid, which can be provided by the energy battery storage systems deployed at the DC link of microgrid PCC. We define such stabilizing resource as stability reserve. The proposed stability reserve is different in nature from the conventional spinning and unspinning operating

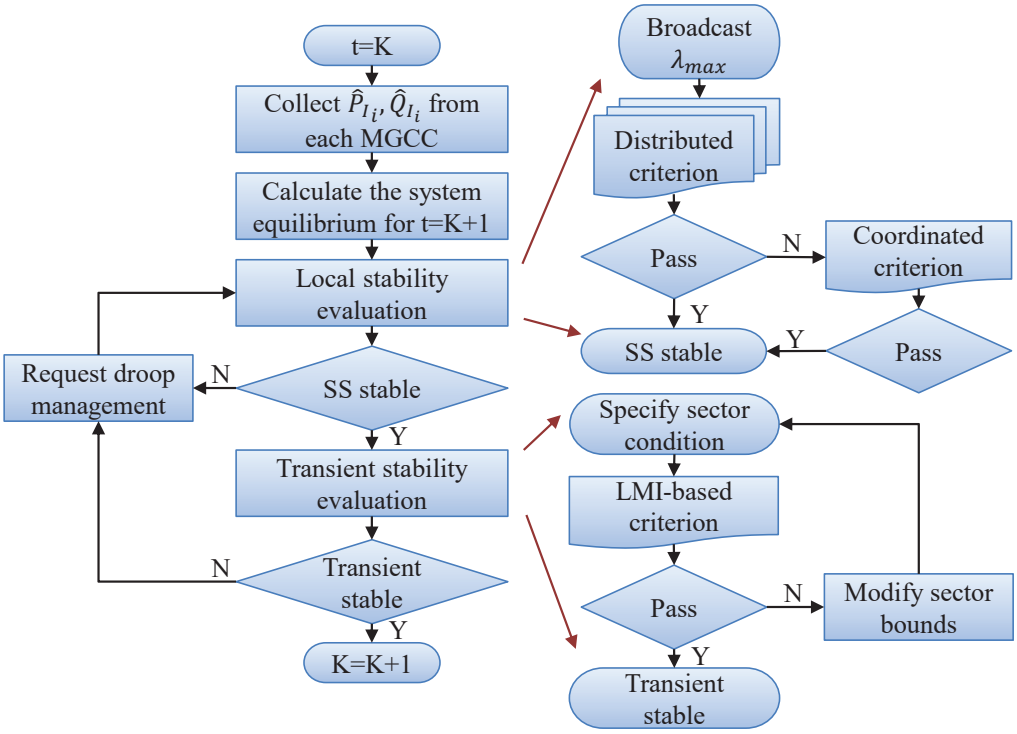

Figure 5.2: Droop management scheme.

reserve. First of all, the conventional operating reserve is the generation capacity available to the system operator within a short interval of time to meet demand in case a generator fail to supply. It is designed to support system operation. However, the proposed stability reserve is for system stabilization purpose provided by the energy storage units in the microgrid to modify its interface droop characteristic. Such stabilizing resources are proposed to guarantee system stability without over-conservative droop gain design for the application scenario that high penetration level of intermittent renewable energy is integrated.

5.3 Tertiary Level Supervisory Control for Microgrid Dispatch

As the highest level of control for multi-microgrid systems, tertiary control is responsible for coordinating the operation of all on-line microgrids [44]. The main

purpose is to mitigate the DER output variation and balance out the long-term mismatch between power production and consumption through aggregation effect, i.e. power exchange among interconnected microgrids. For a reliable, secure and economical operation, the reference setting of each microgrid interface can be managed by the DSO with a supervisory control scheme.

Assume effective power sharing is achieved with the primary level control and system-wide stability guaranteed with the droop management performed at the secondary level. Since distribution lines commonly have comparative resistance and reactance, an ACPF problem is formulated to generate the reference setting for each microgrid. The procedure starts with each microgrid forecasting its total local real and reactive power injection P_I^*, Q_I^* for an operation interval defined by the DSO.

In the ACPF problem formulation, the PCC of the microgrid connected with the external system is designated as the swing bus; PCCs of all the other microgrids will be considered as $P-Q$ buses at the beginning. If the physical limits of V_t is hit for some buses, they will be treated as $P-V$ buses instead.

The ACPF solution $o_e = [\delta_i^*, V_i^*, P_{I_i}^*, Q_{I_i}^*]^T, i = 1 \ldots n$, will be sent to each MGCC for the primary level reference tracking and the secondary level droop management, respectively. It should be noted that the time frame of droop management can be designed differently from the microgrid setting point dispatch resolution. For instance, droop gains for each microgrid may can be managed with a finer resolution for better support of fast variation resources. However, if frequent change of droop gains is not allowed, conservative values can be designed based on the contingency scenarios.

The major difference between the proposed supervisory control and the economic dispatch (ED) program widely used in conventional power systems is that the full set of variables including $\delta_i^*, V_i^*, P_{I_i}^*, Q_{I_i}^*$ will be dispatched to each microgrid interface,

whereas only $V_i^*, P_{I_i}^*$ will be dispatched to each generator in conventional ED problem formulation.

5.4 Management of Multiple Interface VSIs

In current practice of microgrid integration, a single VSI inverter is deployed at the point of common coupling (PCC) as the power electronic interface; however, in the future microgrid-based smart distribution systems, the power rating of each microgrid module could be much larger. For a large utility size microgrid, it is desirable that it can be integrated with the network at multiple connection points (CPs). As by definition, a microgrid acts as a single controllable entity to simplify the interconnection level control implementation. Thus a consistent voltage profile should be guaranteed for all the connection points by the microgrid interface control strategy.

First consider the scenario that at each connection point a physical interface VSI is deployed. For the ith microgrid, assume that there are m CPs each with an interface VSI deployed. Note the real and reactive power injection of the jth VSI as $P_{if_i}^j$, $Q_{if_i}^j$, according to kirchoff's law we have

$$P_{I_i} = \sum_{j=1}^{m} P_{if_i}^j, Q_{I_i} = \sum_{j=1}^{m} Q_{if_i}^j. \tag{5.7}$$

As an example, Fig. 5.3 shows the one-line diagram of a three-microgrid system. Each microgrid is integrated with the network at two distant CPs. The voltage phase angle and magnitude of VSI_1 and VSI_2 can be obtained as

$$\begin{aligned} \delta_{if_1}^1 &= \delta_1^* + \frac{\sigma_{\delta_1}}{\tau_{\delta_1} s + 1}(P_{12}^* - P_{if_1}^1), \\ V_{if_1}^1 &= V_1^* + \frac{\sigma_{V_1}}{\tau_{V_1} s + 1}(Q_{12}^* - Q_{if_1}^1), \end{aligned} \tag{5.8}$$

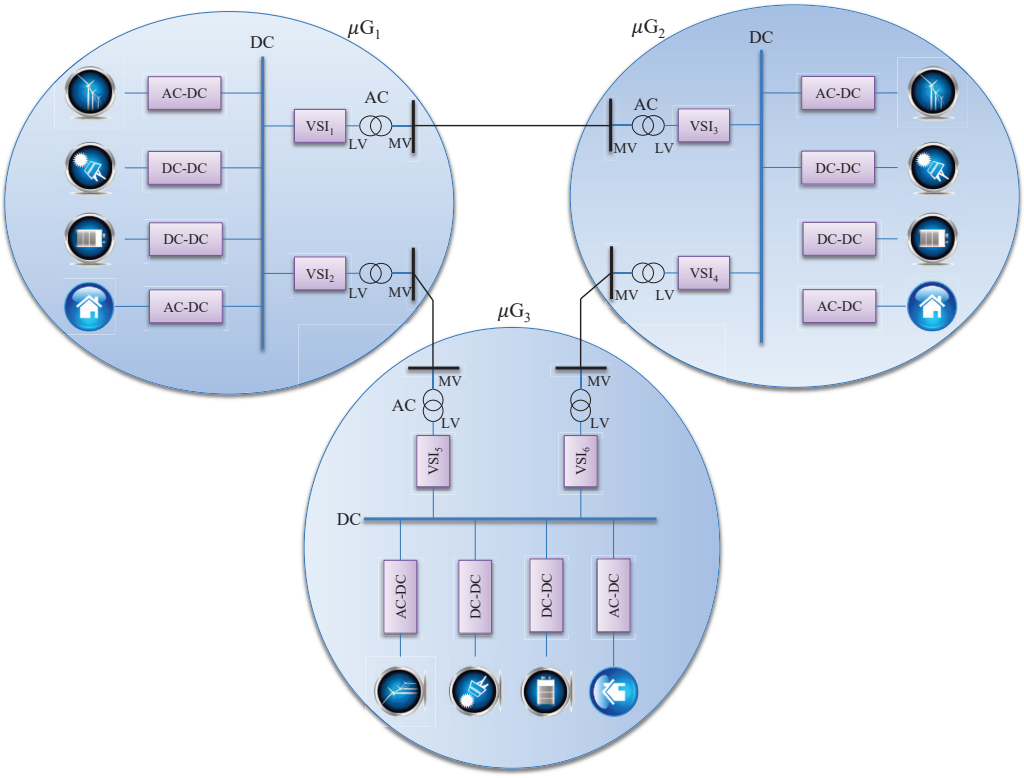

Figure 5.3: A three-microgrid system with multiple connection points.

$$\begin{aligned} \delta_{if_1}^2 &= \delta_1^* + \frac{\sigma_{\delta_1}}{\tau_{\delta_1} s + 1}(P_{13}^* - P_{if_1}^2), \\ V_{if_1}^2 &= V_1^* + \frac{\sigma_{V_1}}{\tau_{V_1} s + 1}(Q_{13}^* - Q_{if_1}^2), \end{aligned} \tag{5.9}$$

where P_{12}^*, Q_{12}^* are the nominal real and reactive branch flow from μG_1 to μG_2. P_{13}^*, Q_{13}^* are the nominal real and reactive branch flow from μG_1 to μG_3. From the power flow solution we have $P_{I_1}^* = P_{12}^* + P_{13}^*$. And from (5.7) we have $P_{I_1} = P_{if_1}^1 + P_{if_1}^2$.

The output terminals of VSI_1 and VSI_2 are equal potential nodes, i.e. $V_{if_1}^1 = V_{if_1}^2 = V_1$, $\delta_{if_1}^1 = \delta_{if_1}^2 = \delta_1$, and thus (5.8) and (5.9) can be combined as

$$\begin{aligned} \tau_{\delta_1}\dot{\delta}_1 + \delta_1 - \delta_1^* &= \sigma_{\delta_1}(P_{I_1}^* - P_{I_1}), \\ \tau_{V_1}\dot{V}_1 + V_1 - V_1^* &= \sigma_{V_1}(Q_{I_1}^* - Q_{I_1}). \end{aligned} \tag{5.10}$$

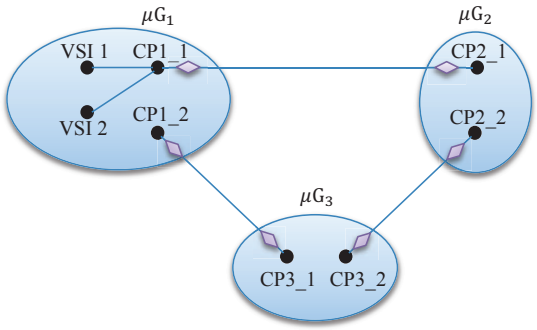

Figure 5.4: Virtual interfacing for a three-microgrid system.

Then (5.10) can be used to represent μG_1 as a single controllable entity.

Now consider the scenario that for some microgrid, the physical integration VSIs are deployed at distant nodes from its CPs. With the algorithm proposed in Section 3.5, the voltage angle and magnitude references can be generated according to (3.19) for virtual interfacing. Fig 5.4 shows a three-microgrid system, in which two integration VSIs are used for virtual interfacing at the connection point CP1_1.

From (5.10) $\delta^1_{if_1}$ and $V^1_{if_1}$ can be calculated, and then according to (3.10) the d and q axis power injection from CP1_1 into the network can be calculated as

$$I_d = \frac{P^1_{if_1}}{V^1_{if_1}},\ I_q = -\frac{Q^1_{if}}{V^1_{if_1}}. \tag{5.11}$$

Assume that we want the d and q axis current to be equally shared between VSI 1 and VSI 2, the d and q axis of each integration VSI will be

$$I_{d_1} = I_{d_2} = 0.5I_d,\ I_{q_1} = I_{q_2} = 0.5I_q. \tag{5.12}$$

Then according to (3.15), the d and q axis output voltage of VSI 1 and 2 can be

calculated

$$\begin{aligned} V_{d_1} &= V_{if_1}^1 + R_1 I_{d_1} - X_1 I_{q_1},\ V_{q_1} = R_1 I_{q_1} + X_1 I_{d_1}, \\ V_{d_2} &= V_{if_1}^1 + R_2 I_{d_2} - X_2 I_{q_2},\ V_{q_2} = R_2 I_{q_2} + X_2 I_{d_2}. \end{aligned} \tag{5.13}$$

From (3.16), the voltage reference for VSI 1 and 2 can be obtained

$$\begin{aligned} V_1^{ref} &= |V_{d_1} + jV_{q_1}|,\ \delta_1^{ref} = \delta_{if_1}^1 + \tan^{-1}(\frac{V_{q_1}}{V_{d_1}}), \\ V_2^{ref} &= |V_{d_2} + jV_{q_2}|,\ \delta_2^{ref} = \delta_{if_1}^1 + \tan^{-1}(\frac{V_{q_2}}{V_{d_2}}). \end{aligned} \tag{5.14}$$

It should be noted that this internal VSI management task should be at a much faster time scale than the tertiary level supervisory control dispatching microgrid interface reference. The reference signals, $V_j^{ref}\angle\delta_j$, $j = 1 \ldots m$, should be dispatched to each VSI with a resolution much higher than the time scale of angle and voltage dynamics. It can be as high as the PMU resolution, e.g. 50Hz, if the local communication is sufficiently fast.

6. NUMERICAL EXAMPLES

6.1 Real Power Sharing Strategies and Virtual Interfacing Scheme

With the proposed angle droop control for real power sharing, better transient performance can be expected compared with the frequency droop-based approaches and strategies emulating synchronous generator behaviour. In conventional power systems, it is well known that local mode oscillations, one generator swings against the rest of the system, are resulted from the second order angle dynamics of the SG swing equations. The corresponding impact is localized to the generator and the line connecting it to the grid. The rest of the system is normally modeled as a constant voltage whose frequency is assumed to remain constant, known as the single machine infinite bus (SMIB) model. On the other hand, the proposed strategy results in a first order angle dynamics without causing such local oscillation.

Fig. 6.1 shows the diagram of a SMIB system, in which a microgrid is connected to an infinite bus through a distribution line with impedance $Z_{12} = 1.5042 + j1.3554\ \Omega$. With the power and voltage based chosen as $V_B = 4.16\ kV$, $S_B = 1\ MVA$ we have the line impedance in per unit $z_{12} = 0.0869 + j0.0783$ p.u.. Assume the infinite bus voltage $V_{inf}\angle\delta_{inf} = 1\angle 0^\circ$ p.u., and the PCC voltage magnitude of microgrid i is fixed at 1 p.u., consider the dynamical response from the initial condition, $V_i\angle\delta_i = 1\angle 0^\circ$ p.u., to the equilibrium point $V_i\angle\delta_i = 1\angle 30^\circ$ p.u.. The corresponding real power injection can be calculated as $P_{I_i} = 3.71$ p.u..

Two interface control strategies are compared with parameters given in Table 6.1, one employing the first order angle droop control, the other emulating synchronous generator behavior, known as the frequency droop with synthetic inertia. Fig. 6.3 shows the trajectories of the PCC voltage angle and real power injection of micro-

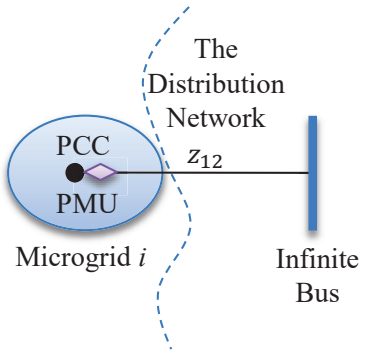

Figure 6.1: One microgrid infinite bus system.

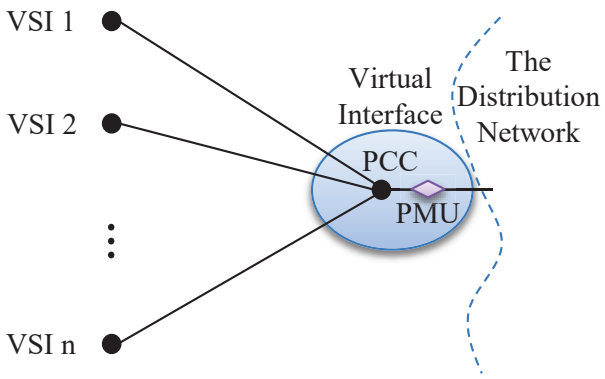

Figure 6.2: Virtual interfacing with internal DER-integration VSIs.

Table 6.1: Interface control parameters.

Parameters	τ_{δ_i}	σ_{δ_i}	Jv_i	Dv_i
Value (p.u.)	5.0	0.5	10	2

grid i. It can be seen that the local oscillation mode presents with the frequency droop method but not with the angle droop control, through which better transient performance can be expected.

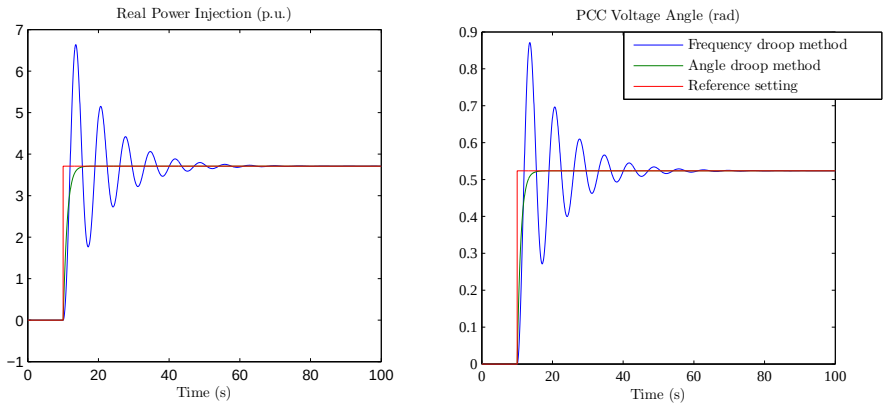

Figure 6.3: PCC voltage and real power injection trajectories.

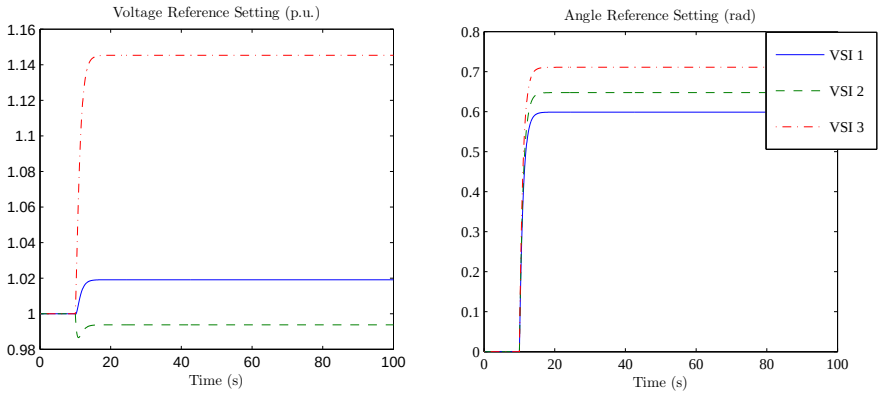

Figure 6.4: Reference setting for DER-integration VSIs.

For the scenario that no physical interface VSI is deployed at the microgrid PCC, diagram shown in Fig. 6.2, the proposed virtual interfacing scheme is adopted managing three DER integration VSIs in a distributed manner. Assume the participation factors for the three VSI $c_{d1} = c_{q1} = c_{d2} = c_{q2} = 0.25$, $c_{d3} = c_{q3} = 0.5$. The electrical distance between each VSI connection point (CP) and the microgrid PCC are

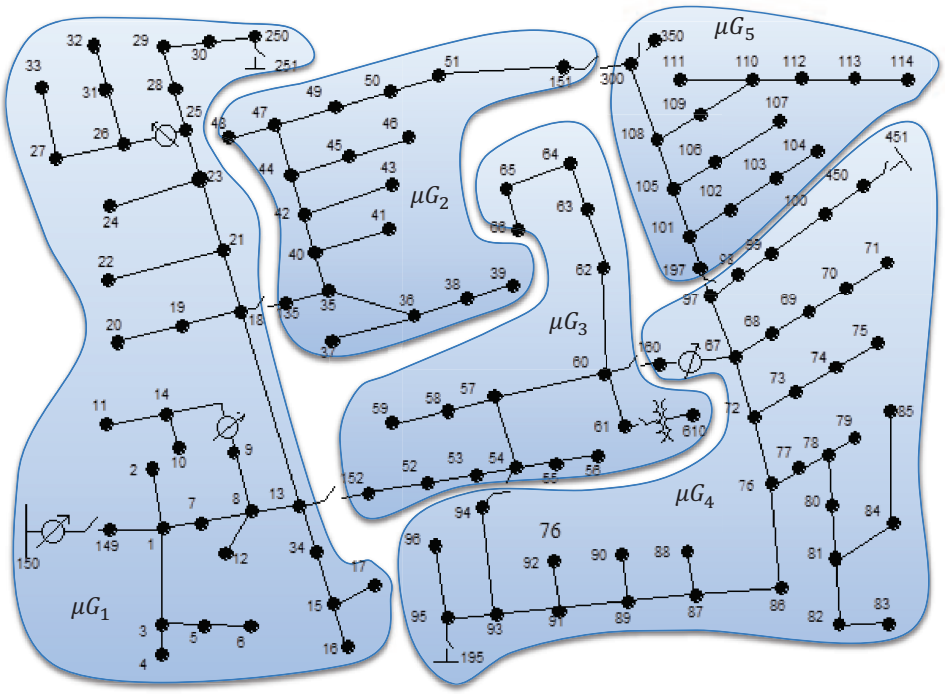

Figure 6.5: Diagram of the study system based on IEEE 123-bus test feeder [60].

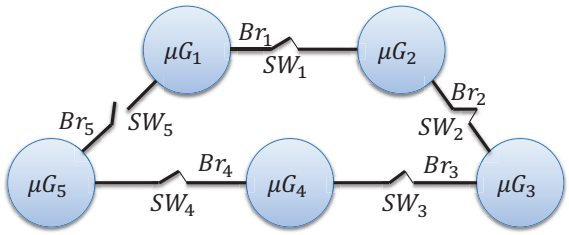

Figure 6.6: Diagram of a 5-microgrid radial system [60].

$z_{e1} = 0.5 + j0.5$, $z_{e2} = 0.5 + j1.0$ and $z_{e3} = 1.0 + j0.5$, respectively. Fig. 6.4 shows the voltage reference setting for each DER-integration VSI, based on which the PCC voltage dynamics as shown in Fig. 6.3 can be obtained.

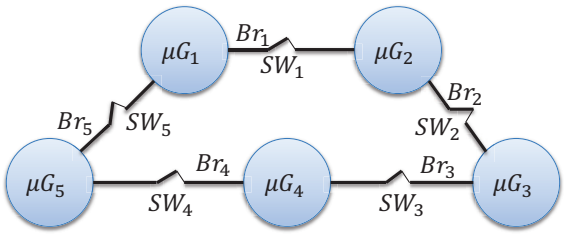

Figure 6.7: Diagram of a 5-microgrid loop system [60].

6.2 Small-signal Stability of Systems with Angle Droop Controlled Interfaces

In this section, we consider a study system designed based on the IEEE 123-node test feeder [26], shown in Fig. 6.5, with some modifications to allow for microgrid application. In current practice, radial distribution systems are more preferred than loop systems by distribution engineers because 1) simple and inexpensive protection schemes can be utilized; 2) fast isolation of faulted section [52]. However, radial distribution systems can have such advantages only if power flows in one direction. In multi-microgrid systems, power exchange among interconnected modules will be dependent on the operating condition of both module at that time. Thus, bi-directional power flow need to be considered. As will be shown in our case study, loop system configurations could be more desirable for multi-microgrid application over the radial ones mainly due to two of their benefits: 1) more balanced power flow (with reduced power loss and better regulated voltage profile); 2) dynamically more secure (allowing for more aggressive droop characteristics for load sharing among interconnected microgrids).

Here we will demonstrate our modeling and DSA framework for both radial and loop system configurations. A 5-microgrid radial system is configured with the default tie-switch status, shown in Fig. 6.6. And also, a loop system is configured by closing all the tie-switches as shown in Fig. 6.7. Here line parameters of the tie-

Table 6.2: Inter-module line parameters

Br No.	1	2	3	4	5
$R(\Omega)$	0.11	0.16	0.05	0.16	0.03
$X(\Omega)$	0.08	0.15	0.03	0.15	0.02

Table 6.3: Module generation and load Profiles

Module	μG_1	μG_2	μG_3	μG_4	μG_5
P_G (kW)	-	600	400	500	800
Q_G (kVar)	-	200	100	400	700
P_L (kW)	920	230	450	270	1530
Q_L (kVar)	470	110	200	120	750

branches are given in Table. 6.2. Aggregated generation and load profiles for each module are given in Table. 6.3.

6.2.1 Load Sharing Loss and Interaction Coefficient

Start with Case A, shown in Fig. 6.6. In this case, 5 microgrids are connected through a radial network. At a specific operation point with the generation and load profiles given in Table. 6.3, PCC voltage profile of each microgrid can be obtained through an AC power flow program, shown in Table. 6.4. In this case, real power loss for load sharing is 9 kW. Here we choose the power base $S_B = 10$ kW and voltage base $V_B = 4.16$ kV. Then the interaction coefficient defined in (4.13) can be calculated as $\lambda^{max} = 0.5671$.

Now consider Case B, shown in Fig. 6.7, in which all tie-switches are closed. Then a loop 5-microgrid system is configured. With the same generation and load profiles as the base case, corresponding PCC profile of each microgrid is obtained as in Table. 6.5. In this case, the real power loss for load sharing reduces to 2 kW, and the interaction coefficient becomes $\lambda^{max} = 0.1424$.

Obviously with the loop configuration, both the real power loss and the interac-

Table 6.4: PCC voltage profile of each microgrid - Case A

PCC	μG_1	μG_2	μG_3	μG_4	μG_5
$V(p.u.)$	1.000	1.000	0.996	0.995	0.987
$\theta(deg.)$	0.000	-0.128	-0.472	-0.559	-0.903

Table 6.5: PCC voltage profile of each microgrid - Case B

PCC	μG_1	μG_2	μG_3	μG_4	μG_5
$V(p.u.)$	1.000	1.003	1.002	1.003	0.999
$\theta(deg.)$	0.000	0.043	0.007	-0.014	-0.045

Table 6.6: Parameter sets of each module

Set	Parameter	μG_1	μG_2	μG_3	μG_4	μG_5
1	J_θ	8.00	12.00	12.00	9.00	12.00
	D_θ	0.29	0.32	0.33	0.29	0.40
	J_V	5.00	2.50	6.25	4.00	4.00
	D_V	0.31	0.25	0.31	0.20	0.25
2	J_θ	8.00	12.0	12.0	9.00	12.0
	D_θ	0.47	0.52	0.55	0.47	0.62
	J_V	10.00	5.00	12.50	8.00	8.00
	D_V	0.63	0.50	0.63	0.40	0.50
3	J_θ	8.00	12.0	12.0	9.00	12.0
	D_θ	1.76	1.60	1.85	1.76	1.90
	J_V	8.60	8.10	8.00	7.65	7.82
	D_V	1.67	1.59	1.54	1.47	1.52

tion coefficient for the system are significantly reduced, by 78% and 75%, respectively. According to the analysis in Section 4.2.2, smaller λ^{max} indicates less damping requirement for module interfaces. Thus more aggressive droop characteristics can be designed for inter-microgrid load sharing, which could be beneficial to support DER integration.

Table 6.7: System-wide stability assessment results

Configuration	Parameter	max Reλ_i	Criterion 1	Criterion 2
Case A	Set 1	0.0231	Unstable	N/A
	Set 2	-0.0189	Stable	N/A
	Set 3	0.1071	Unstable	N/A
Case B	Set 1	-0.0308	Stable	Stable
	Set 2	-0.0497	Stable	Stable
	Set 3	-0.0214	Stable	N/A

6.2.2 Small-signal Stability Assessment

Following the procedure introduced in Section 4.2, system-wide stability can be assessed with the stability criteria derived. Here three sets of interface parameters, shown in Table 6.6, are considered for both radial and loop network configuration Case A and B. System-wide stability is assessed with the coordinated Criterion 1 and distributed Criterion 2, with results given in Table. 6.7. For a specific operation point the assessment procedure starts with module agents evaluating system stability with Criterion 2. If satisfied (Case B, Set 1 and 2), system-wide stability can be concluded. However, if Criterion 2 is not satisfied (Case A, Set 1, 2 and 3; Case B, Set 3), the system coordinator will need to evaluate system-wide stability with Criterion 1. If satisfied, the operation point considered is asymptotically stable (Case A, Set 2; Case B, Set 3); otherwise, instability can be concluded (Case A, Set 1 and 3), which requires module agents to modify their droop gains.

6.3 Transient Stability Assessment and Stability Reserve Management

A 5-microgrid study system is designed based on IEEE 123-node test feeder to demonstrate the proposed transient stability assessment procedure. Fig. 6.8 shows the system partition and Fig. 6.9 shows the one line diagram at the interconnection level when the system is configured as coupling operated microgrids. The tie-branch

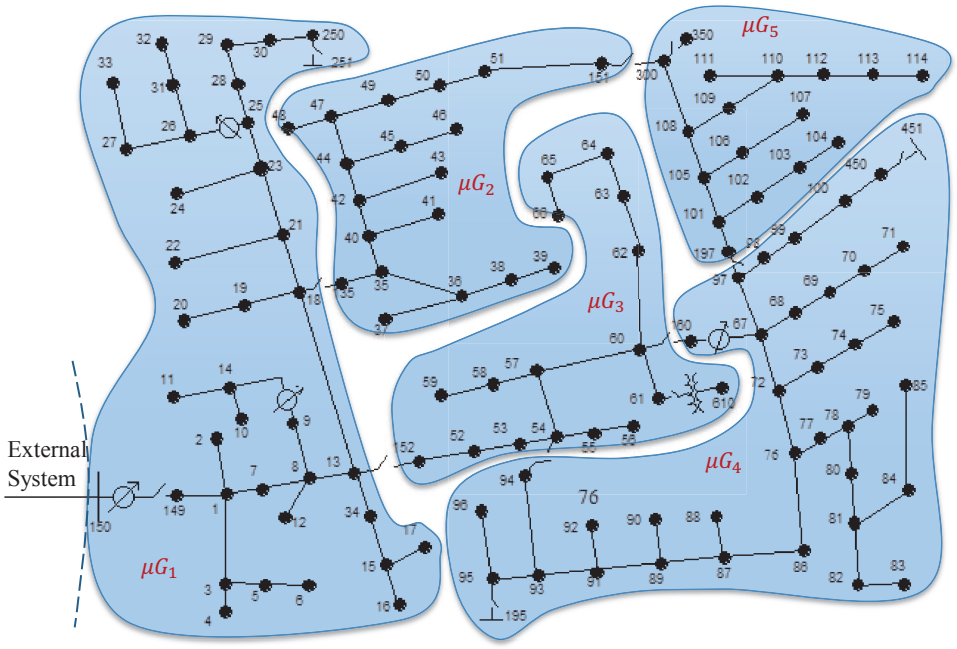

Figure 6.8: Study system based on IEEE 123-node test feeder [62].

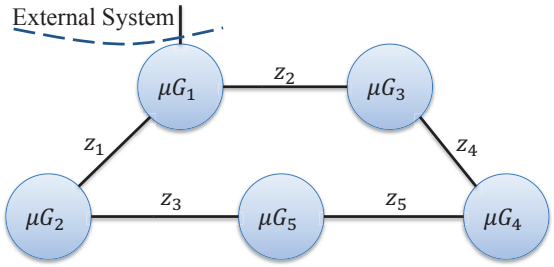

Figure 6.9: Diagram of the 5-microgrid study system.

Table 6.8: Parameters of the tie-branches.

Tie-branch	z1	z2	z3	z4	z5
$R(\Omega)$	1.2030	1.0300	1.4512	1.5042	1.4680
$X(\Omega)$	1.1034	0.7400	1.3083	1.3554	1.1550

parameters are given in Table. 6.8.

Table 6.9: Two consecutive operation points.

PCC	μG_1	μG_2	μG_3	μG_4	μG_5
V^{*K}(p.u.)	1.00	1.00	1.00	1.00	1.00
δ^{*K}(rad)	0.00	-0.38	-0.24	0.34	0.77
V^{*K+1}(p.u.)	1.05	0.95	1.00	1.05	0.95
δ^{*K+1}(rad)	0.00	-0.17	0.03	-0.18	-0.40

Table 6.10: Interface control time constants and droop gains.

Case	Parameter	μG_1	μG_2	μG_3	μG_4	μG_5
A	τ_δ(s)	1.20	1.00	0.80	1.00	1.20
	σ_δ	2%	2%	2%	2%	2%
	τ_V(s)	12.0	10.0	16.0	10.0	12.0
	σ_V	2%	2%	2%	2%	2%
B	τ_δ(s)	1.20	1.00	0.80	1.00	1.20
	σ_δ	15%	15%	15%	15%	20%
	τ_V(s)	12.0	10.0	16.0	10.0	12.0
	σ_V	2%	2%	2%	2%	2%
C	τ_δ(s)	1.20	1.00	0.80	1.00	1.20
	σ_δ	120%	150%	100%	120%	150%
	τ_V(s)	12.0	10.0	16.0	10.0	12.0
	σ_V	2%	2%	2%	2%	2%

6.3.1 Transient Stability Assessment

In this section, the transient stability of the study system will be evaluated starting from the initial condition o^K to the next operation point o^{K+1} given in Table. 6.9.

In order to study the impact of microgrid droop gain settings on system stability, three study cases are formulated. The interface control time constants and droop gains for each microgrid are given in Table. 6.10.

The local stability of o^{K+1} can be evaluated with the small signal model (4.4) formulated in Section 4.1. The system eigenvalues for each study case are plotted in Fig. 6.10. For Case A and B, the system equilibrium o^{K+1} is small signal stable since

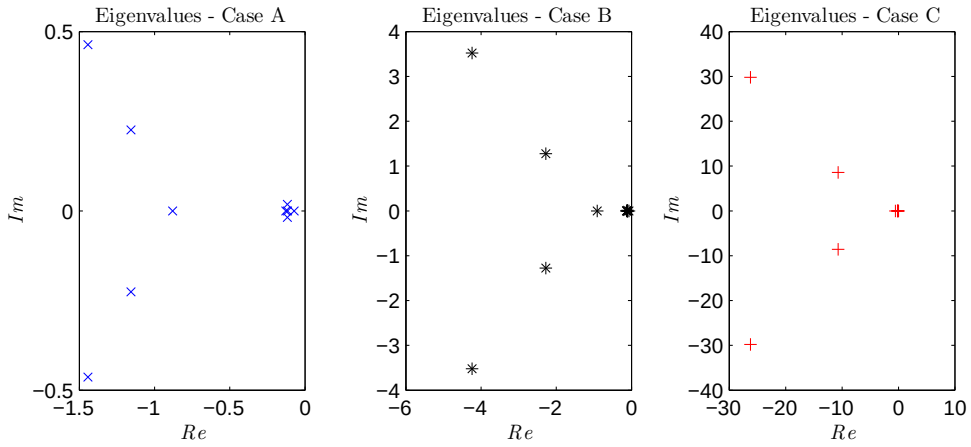

Figure 6.10: Eigenvalues for small signal system model.

all the eigenvalues have negative real parts. For Case C, the system equilibrium o^{K+1} is small signal unstable with a positive eigenvalue 0.0014. Obviously, with smaller interface droop gains the system tends to have better stability feature.

Now that the system equilibrium o^{K+1} is small signal stable for Case A and B, transient stability from the initial condition $o^K = (V^{*K}, \delta^{*K})$ to the intermediate point o^{K+} need to be evaluated according to the assessment framework in Fig.4.2.

With the assessment procedure given in Section 4.2, the transient stability feature can be evaluated for Case A and B, given in Table 6.11. For Case A, the LMIs formulated in (4.31) are feasible with the sector condition $\phi_j(y_j) \in [-1, 1]$, $j = 1 \dots 10$, thus global stability can be concluded. For Case B, feasible solution of (4.31) cannot be obtained with sector condition $\phi_j(y_j) \in [-1, 1]$, $j = 1 \dots m$, whereas regional stability can be established with sector condition $\phi_j(y_j) \in [0, 1]$, $j = 1 \dots 10$. The corresponding stability region is given in Table. 6.12, in which $x_i = \delta_i^{*K} - \delta_i^{*K+1}, i = 1 \dots 5$. From Table. 6.9, we have $x_1 - x_2 = 0.21$, $x_1 - x_3 = 0.27$, $x_2 - x_5 = -1.38$, $x_3 - x_4 = -0.79$, $x_4 - x_5 = -0.65$. Clearly, the initial condition o^K falls into the stability region of o^{K+}, thus transient stability can be concluded for Case B.

Table 6.11: Stability assessment results.

Stability	Case A	Case B	Case C
o^{K+1} (small-signal)	Stable	Stable	Unstable
$o^K \rightarrow o^{K+}$ (Transient)	Globally stable	Regionally stable	-

Table 6.12: Transient stability region.

Angle bound	$x_1 - x_2$	$x_1 - x_3$	$x_2 - x_5$	$x_3 - x_4$	$x_4 - x_5$
Upper bound (rad)	1.14	1.30	1.07	1.06	0.95
Lower bound (rad)	-1.82	-1.19	-1.87	-1.87	-1.72

6.3.2 Stability Reserve and Droop Management

Stability reserve can be configured to manage the droop gains of each microgrid interface. For a specific system operation condition, model reference tracking can be performed the MGCC by controlling its stability reserve.

We know that the operation point o^{K+1} is small signal unstable if the plant model of each microgrid interface has the droop gains specified as in Table. 6.10 - Case C; whereas transient stability can be established with the Case A and B droop gains. Design the reference model of each microgrid with Case A droop gains, and consider the scenario that starting from the initial condition o^K, each MGCC spent 10s for their reserved to be committed. The system can be stabilized through controlling the stability reserve of each microgrid. As can be seen from the time domain simulation result plotted in Fig. 6.11, the system states $\Delta\delta$, ΔV and interaction variables ΔP_I, ΔQ_I start converging to zero when the stability reserves are committed at 10s.

Fig. 6.12 shows the response of the stability reserve of each microgrid, from which we can observe that P_R of each microgrid converge to zero at the steady state. Such

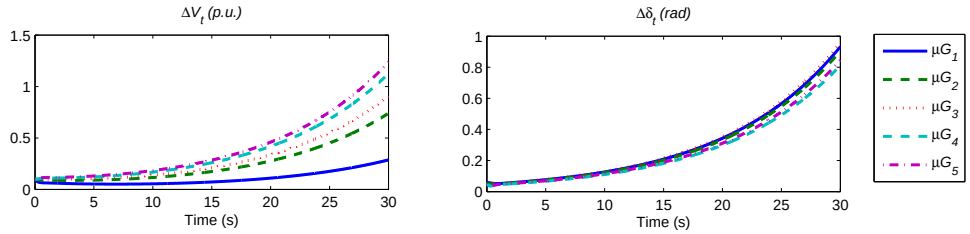

Figure 6.11: Time domain simulation results - Case C plant model, Case A reference model.

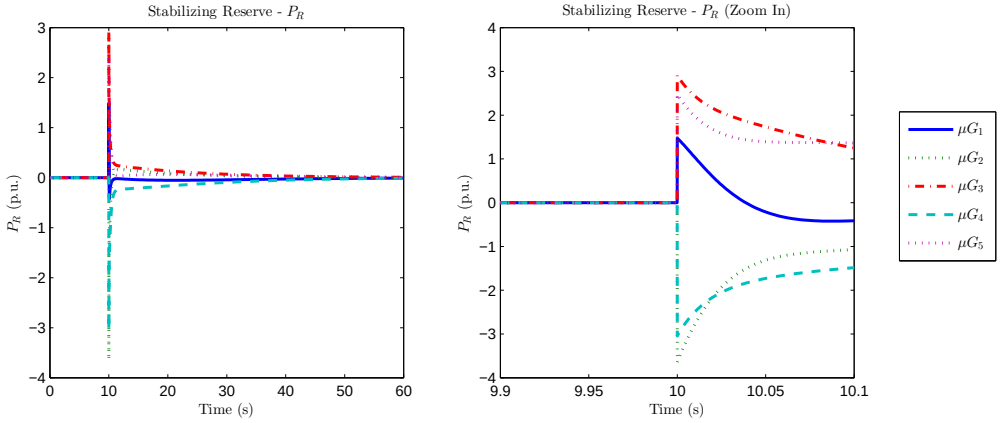

Figure 6.12: The stability reserve responses - Case C plant model, Case A reference model.

phenomena are consistent with our theoretical analysis since

$$P_{R_i} = -l_{P_i} \Delta P_{I_i}, \tag{6.1}$$

At the steady state $\Delta\delta_i(\infty) = 0$, $\Delta V_i(\infty) = 0$, $i = \ldots n$, then according to (4.4) and (4.5) we have,

$$P_{R_i}(\infty) = -l_{P_i} \Delta P_{I_i}(\infty) = 0. \tag{6.2}$$

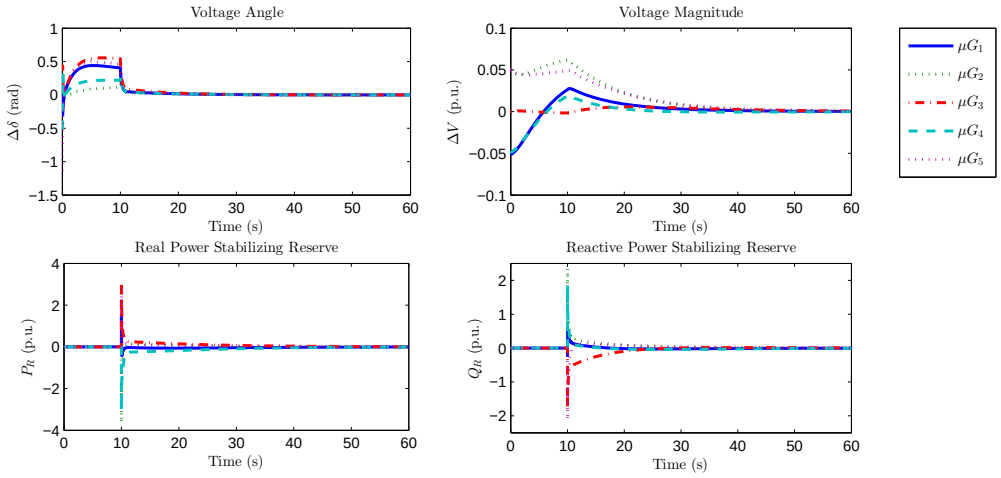

Figure 6.13: The stability reserve responses - Case C plant model, 1% reference model voltage droop.

Table 6.13: Inter-module line parameters

TB No.	1	2	3	4	5
$R(\Omega)$	1.0300	1.4680	1.5042	1.4512	1.2030
$X(\Omega)$	0.7400	1.1150	1.3554	1.3083	1.1034

In the study case above only real power reserve is configured. Actually, reactive power reserve can be used for voltage droop management with the control law given in (5.3). Now consider the scenario that the microgrid interface plants have Case C parameters and the corresponding reference models have the same τ_δ, σ_δ, and τ_V as in Case A, but with $\sigma_V = 1\%$ for each microgrid interface. The response of system states $\Delta\delta$, ΔV and the stability reserves P_R, Q_R are plotted in Fig. (6.13), from which we see that all these variables approach zero at the steady state.

6.4 Hierarchical Control Framework

In this section, a study system designed based on IEEE 123-node test feeder, shown in Fig. 6.14, will be used to demonstrate the feasibility of the proposed

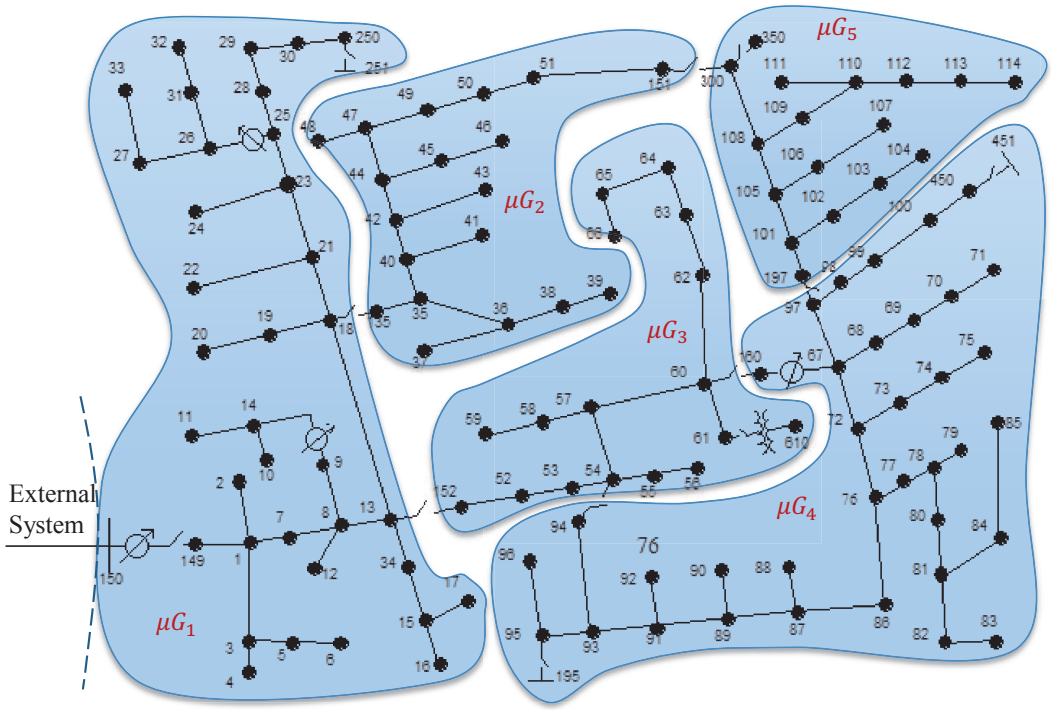

Figure 6.14: Study system based on IEEE 123-node test feeder [62].

interactive control framework. Configured as a microgrid-based distribution system, 5 microgrids are interconnected through tie-branches (TBs), with line parameters given in Table. 6.13.

In each microgrid, various energy sources are configured including wind farm, solar system, natural gas generators and etc, of which the aggregation will be the $P_{G_i}, Q_{G_i}, i = 1 \dots 5$ in our problem formulation. Local load includes residential, commercial and industrial customers, of which the aggregation will be the $P_{L_i}, Q_{L_i}, i = 1 \dots 5$. And also, utility-scale battery energy storage system is deployed in each microgrid serving as the regulation power $P_{R_i}, Q_{R_i}, i = 1 \dots 5$.

6.4.1 System Operating Condition and Interaction Coefficient

With the ACPF problem formulated in Section 5.3 solved every 15 minutes, the system operating condition and the corresponding reference setting point for each microgrid can be obtained. Here nine consecutive operation points are presented in Fig. 6.15. The corresponding generation and load profile of each microgrid is given in Table 6.14.

Detailed generation and load profile is given in the appendix. Corresponding to each system operating condition, the interaction coefficient λ_{max} defined in (4.13) can be calculated, as plotted in Fig. 6.16. In Fig. 6.15 per unit representation (p.u.) are used for V_t^*, P_I^* and Q_I^*, except for θ_t^* radian measure is used. The voltage and power bases are $V_B = 4.16$ kV, $S_B = 1$ MW, respectively.

The interaction coefficient shows the network stressfulness at a specified operation point. It can be seen from Fig. 6.15, 6.16 that the higher utilization of the tie-branches for power exchange the larger interaction coefficient will the system have. For the operation point at 30 min, the largest real power branch flow is $F_{2-1} = 0.31$ MW from μG_2 to μG_1 through TB_5. The corresponding interaction coefficient $\lambda_{max}(15) = 0.008$. For the operation point at 60 min, the largest real power branch flow is $F_{1-3} = 3.58$ MW from μG_1 to μG_3 through TB_1. The corresponding interaction coefficient $\lambda_{max}(60) = 1.316$. Apparently, the system interaction coefficient at 60 min is much larger than that at 30 min with significantly higher utilization of the network for power exchange.

6.4.2 Droop Gain and System-wide Stability

As discussed in Section 4.2.2, droop gains of each microgrid interface need to satisfy the criterion in (4.14) so that the system-wide small signal stability can be guaranteed. Start with the scenario that no real time droop management is per-

Table 6.14: Generation and load profile for each microgrid (in per unit).

OP	Composition	μG_1	μG_2	μG_3	μG_4	μG_5
	P_G	0.40	0.60	1.50	0.30	0.30
1	Q_G	0.14	0.27	-0.22	-0.33	0.09
$t = 0$	P_L	0.13	0.20	2.50	0.10	0.10
	Q_L	0.02	0.03	0.02	0.03	0.01
	P_G	0.63	0.15	0.90	0.60	0.90
2	Q_G	-0.50	0.09	-0.11	0.18	0.27
$t = 15$	P_L	1.05	0.05	1.50	0.20	0.30
	Q_L	0.04	0.01	0.01	0.02	0.03
	P_G	0.43	0.45	0.30	0.15	0.15
3	Q_G	-0.10	0.18	-0.11	0.09	-0.11
$t = 30$	P_L	0.72	0.15	0.50	0.05	0.05
	Q_L	0.01	0.02	0.01	0.01	0.01
	P_G	2.55	0.90	1.80	0.15	1.20
4	Q_G	-0.82	0.27	0.09	0.09	0.36
$t = 45$	P_L	0.85	0.30	3.00	0.25	2.00
	Q_L	0.07	0.03	0.01	0.01	0.04
	P_G	8.63	0.30	3.00	0.30	3.00
5	Q_G	-4.01	0.54	1.80	0.72	1.80
$t = 60$	P_L	2.88	0.10	5.00	0.10	5.00
	Q_L	0.36	0.06	0.20	0.08	0.20
	P_G	4.71	0.15	1.80	0.90	1.20
6	Q_G	-0.93	-0.11	1.08	0.27	-0.22
$t = 75$	P_L	1.57	0.25	3.00	1.50	2.00
	Q_L	0.08	0.01	0.12	0.03	0.02
	P_G	3.14	0.75	0.90	1.50	0.30
7	Q_G	-0.16	-0.22	0.09	0.27	0.09
$t = 90$	P_L	1.05	1.25	1.50	2.50	0.10
	Q_L	0.01	0.02	0.01	0.03	0.01
	P_G	1.30	0.30	0.30	0.30	0.90
8	Q_G	-0.27	-0.11	0.09	0.09	0.18
$t = 105$	P_L	0.43	0.50	0.10	0.50	1.50
	Q_L	0.02	0.01	0.01	0.01	0.02
	P_G	0.07	0.30	0.75	0.30	1.20
9	Q_G	-0.61	0.09	0.18	-0.11	0.36
$t = 120$	P_L	0.11	0.10	0.25	0.10	2.00
	Q_L	0.06	0.01	0.02	0.01	0.04

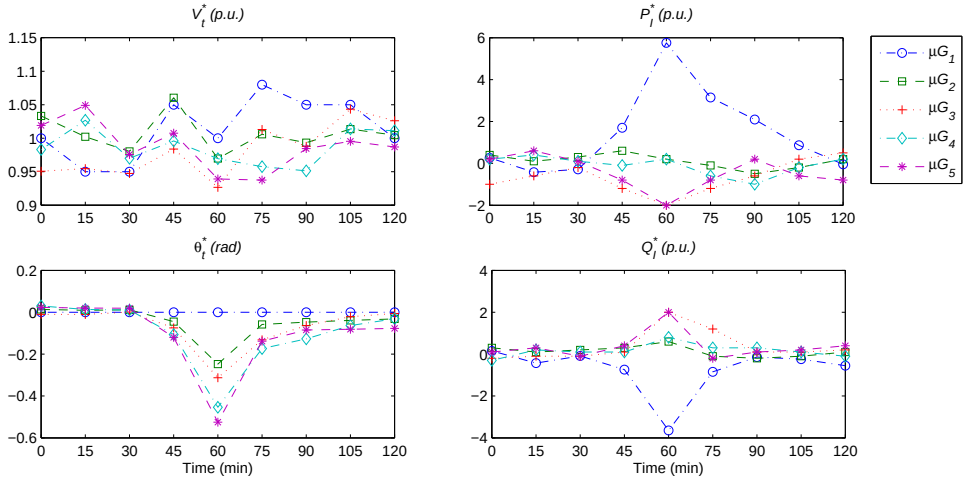

Figure 6.15: Nine consecutive operation points of each microgrid [62].

formed. Each microgrid interface VSI has its droop gain designed a priori without considering system operating condition, i.e. the plant model (3.4), (3.8) will be used to represent the interface control dynamics.

To match the reference setting P_I^*, Q_I^*, let

$$P_R = P_I^* + P_L - P_G,\ Q_R = Q_I^* + Q_L - Q_G. \tag{6.3}$$

Then together with (3.4) and (3.8) we have

$$\begin{aligned} \Delta\dot{\delta} &= -\frac{1}{\tau_\delta}\Delta\delta - \frac{\sigma_\delta}{\tau_\delta}\Delta P_I, \\ \Delta\dot{V} &= -\frac{1}{\tau_V}\Delta V - \frac{\sigma_V}{\tau_V}\Delta Q_I. \end{aligned} \tag{6.4}$$

With each microgrid interface dynamics represented as in (6.4), the entire 5-microgrid system can be modeled following the procedure described in Section 4.1.

Assume the plant model parameters are uniformly designed for each microgrid interface, as given in Table. 6.15.

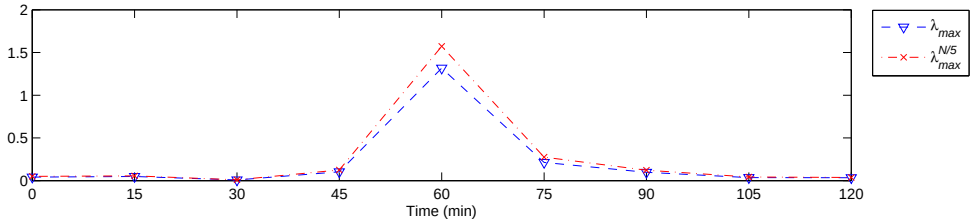

Figure 6.16: Variation of the system interaction coefficient [62].

Table 6.15: Interface plant model parameters

Parameter	τ_δ	σ_δ	τ_V	σ_V
Value	8.0	2.0	4.0	2.0

Table 6.16: System operation point at 60 min

State	μG_1	μG_2	μG_3	μG_4	μG_5
$V_t^*(p.u.)$	1.0000	0.9698	0.9267	0.9695	0.9392
$\delta_t^*(rad)$	0.0000	-0.2478	-0.3130	-0.4540	-0.5252
$P_I^*(p.u.)$	5.7563	0.2000	-2.0000	0.2000	-2.0000
$Q_I^*(p.u.)$	-3.6458	0.6000	2.0000	0.8000	2.0000

Time domain simulation is performed the obtained system model for the operation point at 60 min, as presented in Table. 6.16 (worst case scenario). With the initial condition $\Delta V_{t_i} = 0.10$, $\Delta\delta_{t_i} = 0.05$, $i = 1 \ldots 5$, system response for the first 30 seconds is shown in Fig. 6.17, from which we see that the system is unstable as the state trajectories do not converge to their reference values.

Now consider the scenario that real time droop gains of each microgrid interface are managed interactively with the DSO through the procedure introduced in Section 5.2. Assume for each module, the PCC voltage phase angle and magnitude are required to be regulated within $\pm 5^\circ$ ($\pm 0.0873 rad$), $\pm 0.05 p.u.$ from their reference values, respectively. According to the criterion in (4.14), the regulation capacity of

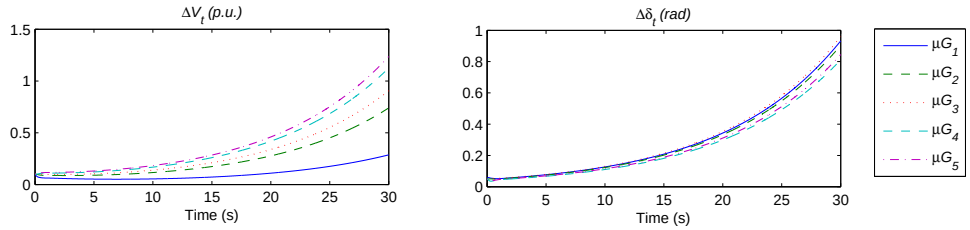

Figure 6.17: System state trajectories without droop management.

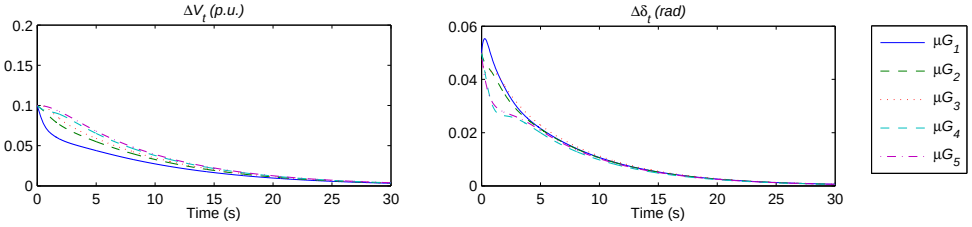

Figure 6.18: System state trajectories with interactive droop management.

each microgrid needs to be configured satisfying

$$\begin{aligned} P_{R_i}^{up} = P_{I_i}^{dn} &> 0.0873\lambda_{max}, \\ Q_{R_i}^{up} = Q_{I_i}^{dn} &> 0.05\lambda_{max}. \end{aligned} \tag{6.5}$$

For the operation point at 60 min, presented in Table. 6.16, the system interaction coefficient $\lambda_{max}(60) = 1.316$. Then without loss of generality, assume the regulation capacity is uniformly configured for each microgrid as

$$\begin{aligned} P_{R_i}^{up} = P_{I_i}^{dn} &= 0.16(p.u.), \\ Q_{R_i}^{up} = Q_{I_i}^{dn} &= 0.08(p.u.). \end{aligned} \tag{6.6}$$

Choosing a 10% margin, i.e. $m_V = m_\delta = 0.1$, the droop gains of each microgrid can be determined as follows,

$$\begin{aligned} \sigma_{\delta_r} &= 0.49, \\ \sigma_{V_r} &= 0.56. \end{aligned} \tag{6.7}$$

Assume successful reference tracking is achieved with the MRC-based primary level control, the designed droop gains $\sigma\delta_r$, σV_r are used instead of the plant droop gains σ_δ, σ_V to represent microgrid interface dynamics. Keep the time constants unchanged $\tau_{\delta_r} = \tau_\delta = 8.0$, $\tau_{V_r} = \tau_V = 4.0$, and consider the same system operation point at 60 min with the same initial condition specified above, the system state trajectories are obtained, shown in Fig. 6.18. It can be observed that the system is asymptotically stable as the state trajectories converge to their reference values at steady state.

7. CONCLUSION

7.1 Summary

In this work, a novel control framework for multi-microgrid systems is formulated. Revolutionary changes are expected in future distribution grid to support distributed/renewable energy integration. More active, intelligent and reliable behaviors are envisioned in future distribution systems, which requires new design of both the system architecture and control framework. The concept of microgrid had been proposed to formulate a local energy cluster that packaging closely located sources and loads at the point of common coupling (PCC). For the upper level system control and management, each microgrid presents to the macro grid as a single controllable entity. Such system architecture is quite promising in realizing the desirable smart grid functions in a simplified manner.

Even with nicely clustered system architecture, many important technical challenges need to be solved. First of all, appropriate power sharing among coupling operated microgrids need to be achieved. Moreover, unlike conventional power systems employing synchronous generators as dynamical interface handling operational disturbance and uncertainty, voltage source inverters (VSIs) are commonly utilized in microgrids for grid connection. Proper interface behavior of those VSIs is desirable to provide effective dynamical support to the system. A novel interface control strategy is proposed in this work to address the aforementioned problems.

Another challenge comes with the intermittent nature of distributed/renewable generation. With high penetration of DERs, the operating condition of multi-microgrid systems can vary in a much wider range in a much shorter term compared with large multi-machine systems. In order to achieve sustainable operation,

hierarchical control is employed for large multi-machine systems, in which the control parameters are designed based on the worst case scenario (WCS) predicted in the planning phase. However, for multi-microgrid systems with operating condition changing dramatically, the WCS approach will result in over-conservative design.

For the novel system architecture, the hierarchical control strategy needs to be redesigned to allow for high DER penetration. To avoid the over-conservativeness issue, a model reference control (MRC)-based scheme is proposed for online droop gain tuning at the primary level. Conservativeness can be significantly reduce by tuning the interface control parameters in a timely manner according to updated system operating condition.

At the secondary level, a droop gain management scheme is proposed. The droop gains of the reference model to be tracked by the primary level control will be determined based on the small-signal and transient stability assessment result. Obviously, this scheme is fundamentally different from the secondary level frequency control performed in convention multi-machine systems aiming at eliminating steady state frequency deviation from the nominal value. We have shown in our analysis that with angle droop method employed in the interface control, the frequency deviation approaches zero at the steady state, thus there is no need to perform secondary level frequency control.

At the tertiary level, an AC-power flow based supervisory control scheme is proposed for microgrid dispatch. Different from the conventional economic dispatch program, the full set of the power flow solution V^*, δ^*, P_I^* and Q_I^* will be dispatched to each microgrid interface. Thanks to the synchrophasor measurement (PMU), exact power flow management becomes possible with this scheme.

7.2 Future Work

In the future work, demand side management will be studied. The key idea is to extend this approach to the scenario that a distribution grid is configured as an interconnection of both microgrids and dynamical responsive loads. Responding to different signals, load component in each demand response (DR) category will provide dynamical support to the system on different aspects.

With PMU deployed at the load bus/node, responsive load components can be controlled to respond to different indication signals. Fig. 1 shows the complete signal-processing model of the state of the art PMU. Signals that can serve as good power imbalance indicators include 1) voltage angle, 2) frequency - Freq, 3) derivative of frequency ROCOF, 4) voltage magnitude. The first three can be used as real power response indicator, while the last one as reactive power response indicator. The derivative of voltage magnitude, although not directly reported, can be easily calculated from the voltage magnitude, which can also be used as reactive power response indicator.

Responding to different signals, the responsive load can be classified into the following categories.

- Non-responsive load. Loads in this class do not respond to any indicator signal, which can be modeled as constant power load in system dynamical studies:

$$P_{L_N} = P^*_{L_N}, Q_{L_N} = Q^*_{L_N}.$$

- Load responding to voltage angle. Loads in this class are real power loads responding to the voltage phase angle of the load bus/node with respect to the

synchronized reference dispatched by the DSO:

$$P_{L_A} = P^*_{L_A} - \frac{1}{\sigma_\delta}(\delta_L - \delta^*_L).$$

- Load responding to frequency. Loads in this class are real power loads responding to the load bus/node frequency ω_L with respect to the nominal frequency ω_0:

$$P_{L_F} = P^*_{L_F} - \frac{1}{\sigma_\omega}\Delta\omega_L,$$

where $\Delta\omega_L = \omega_L - \omega_0$.

- Load responding to ROCOF. Loads in this class are real power loads providing inertia support and responding to the voltage phase angle of the load bus/node frequency:

$$P_{L_R} = P^*_{L_R} - J_L\dot{\omega}_L.$$

- Load responding to voltage magnitude. Loads in this class are reactive power loads responding to the voltage magnitude of the load bus/node with respect to the reference dispatched by the DSO:

$$Q_{L_V} = Q^*_{L_V} - \frac{1}{\sigma_V}(V_L - V^*_L).$$

- Load responding to the derivative of voltage magnitude. Loads in this class are reactive power loads responding to the derivative of the load bus/node voltage

magnitude:

$$Q_{L_C} = Q^*_{L_C} - K_V \dot{V}_L.$$

As an aggregation of all the load classes, the dynamical behavior of a load bus/node can be modeled as follows.

$$\begin{aligned} \dot{\delta}_L &= \Delta\omega_L, \\ J_L\dot{\omega_L} + \frac{1}{\sigma_\omega}\omega_L + \frac{1}{\sigma_\delta}(\delta_L - \delta^*_L) &= P^*_L - P_L, \\ K_V\dot{V_L} + \frac{1}{\sigma_V}(V_L - V^*_L) &= Q^*_L - Q_L, \end{aligned}$$

where $P^*_L = P^*_{L_N} + P^*_{L_A} + P^*_{L_F} + P^*_{L_R}$, $Q^*_L = Q^*_{L_N} + Q^*_{L_V} + P^*_{L_C}$, $P_L = P_{L_N} + P_{L_A} + P_{L_F} + P_{L_R}$, $Q_L = Q_{L_N} + Q_{L_V} + P_{L_C}$.

Then a load module can provide similar dynamical support as the microgrid interface by managing the real and reactive power load P_L, Q_L instead of directly controlling the voltage and angle profile $V_L\angle\delta_L$.

If a load module is so aggregated that the bottom-up load modeling approach requires critical data collection, computation and communication. Data-driven method can be a good alternative to perform a top-down model identification.

REFERENCES

[1] Peter Asmus, Adam Cornelius, and Clint Wheelock. Microgrids–islanded power grids and distributed generation for community, commercial, and institutional applications. *Pike research*, 2009.

[2] Fo N Bailey. The application of lyapunov's second method to interconnected systems. *Journal of the Society for Industrial & Applied Mathematics, Series A: Control*, 3(3):443–462, 1965.

[3] Arthur R Bergen and Vijay Vittal. *Power systems analysis*. Pearson Education India, 2009.

[4] Steve Bossart. Doe perspective on microgrids. In *Advanced Microgrid Concepts and Technologies Workshop*, 2012.

[5] H Bourles, F Colledani, and MP Houry. Robust continuous speed governor control for small-signal and transient stability. *Power Systems, IEEE Transactions on*, 12(1):129–135, 1997.

[6] Stephen P Boyd, Laurent El Ghaoui, Eric Feron, and Venkataramanan Balakrishnan. *Linear matrix inequalities in system and control theory*, volume 15. SIAM, 1994.

[7] Shin-Ju Chen and Jong-Lick Lin. Maximal stability bounds of singularly perturbed systems. *Journal of the Franklin Institute*, 336(8):1209–1218, 1999.

[8] Yong Chen, Ralf Hesse, Dirk Turschner, and Hans-Peter Beck. Improving the grid power quality using virtual synchronous machines. In *Power engineering, energy and electrical drives (POWERENG), 2011 international conference on*, pages 1–6. IEEE, 2011.

[9] Uthier Delille, Bruno Francois, and Gilles Malarange. Dynamic frequency control support by energy storage to reduce the impact of wind and solar generation on isolated power system's inertia. *Sustainable Energy, IEEE Transactions on*, 3(4):931–939, 2012.

[10] RC Dugan, RF Arritt, TE McDermott, SM Brahma, and K Schneider. Distribution system analysis to support the smart grid. In *Power and Energy Society General Meeting, 2010 IEEE*, pages 1–8. IEEE, 2010.

[11] Erik Ela, Michael Milligan, and Brendan Kirby. Operating reserves and variable generation. *Contract*, 303:275–3000, 2011.

[12] DNV GL Energy. A review of distributed energy resources, 2014.

[13] Fang Gao and M Reza Iravani. A control strategy for a distributed generation unit in grid-connected and autonomous modes of operation. *Power Delivery, IEEE Transactions on*, 23(2):850–859, 2008.

[14] F Gonzalez-Longatt, E Chikuni, and E Rashayi. Effects of the synthetic inertia from wind power on the total system inertia after a frequency disturbance. In *Industrial Technology (ICIT), 2013 IEEE International Conference on*, pages 826–832. IEEE, 2013.

[15] Josep M Guerrero, Juan C Vasquez, José Matas, Luis García de Vicuña, and Miguel Castilla. Hierarchical control of droop-controlled ac and dc microgridsa general approach toward standardization. *Industrial Electronics, IEEE Transactions on*, 58(1):158–172, 2011.

[16] Wassim M Haddad, Vikram Kapila, and Vijaya-Sekhar Chellaboina. Guaranteed domains of attraction for multivariable luré systems via open lyapunov

surfaces. *International Journal of Robust and Nonlinear Control*, 7(10):935–949, 1997.

[17] Stanley H Horowitz, Arun G Phadke, Bruce Renz, et al. The future of power transmission. *Power and Energy Magazine, IEEE*, 8(2):34–40, 2010.

[18] Eklas Hossain, Ersan Kabalci, Ramazan Bayindir, and Ronald Perez. Microgrid testbeds around the world: State of art. *Energy Conversion and Management*, 86:132–153, 2014.

[19] Garng M Huang, Liang Zhao, and Xuefeng Song. A new bifurcation analysis for power system dynamic voltage stability studies. In *Power Engineering Society Winter Meeting, 2002. IEEE*, volume 2, pages 882–887. IEEE, 2002.

[20] Marija D Ilic and John Zaborszky. *Dynamics and control of large electric power systems*. Wiley New York, 2000.

[21] Petros A Ioannou and Jing Sun. *Robust adaptive control*. Courier Dover Publications, 2012.

[22] Shivkumar V Iyer, Madhu N Belur, and Mukul C Chandorkar. A generalized computational method to determine stability of a multi-inverter microgrid. *Power Electronics, IEEE Transactions on*, 25(9):2420–2432, 2010.

[23] F Katiraei and MR Iravani. Power management strategies for a microgrid with multiple distributed generation units. *Power Systems, IEEE Transactions on*, 21(4):1821–1831, 2006.

[24] F Katiraei, MR Iravani, and PW Lehn. Small-signal dynamic model of a microgrid including conventional and electronically interfaced distributed resources. *Generation, Transmission & Distribution, IET*, 1(3):369–378, 2007.

[25] Faridaddin Katiraei, Mohammad Reza Iravani, and PW Lehn. Micro-grid autonomous operation during and subsequent to islanding process. *Power Delivery, IEEE Transactions on*, 20(1):248–257, 2005.

[26] WH Kersting. Radial distribution test feeders. *Power Systems, IEEE Transactions on*, 6(3):975–985, 1991.

[27] Sung-Hun Ko, Seong R Lee, Hooman Dehbonei, and Chemmangot V Nayar. Application of voltage-and current-controlled voltage source inverters for distributed generation systems. *Energy Conversion, IEEE Transactions on*, 21(3):782–792, 2006.

[28] Petar Kokotovic, Hassan K Khalil, and John O'reilly. *Singular perturbation methods in control: analysis and design*, volume 25. Siam, 1999.

[29] Prabha Kundur, Neal J Balu, and Mark G Lauby. *Power system stability and control*, volume 7. McGraw-hill New York, 1994.

[30] Peter Lancaster and Miron Timor Tismenetsky. *The theory of matrices: with applications*. Academic Pr, 1985.

[31] Robert H Lasseter. Smart distribution: Coupled microgrids. *Proceedings of the IEEE*, 99(6):1074–1082, 2011.

[32] David M Laverty, D John Morrow, Robert Best, and PA Crossley. Internet based phasor measurement system for phase control of synchronous islands. In *Power and Energy Society General Meeting-Conversion and Delivery of Electrical Energy in the 21st Century, 2008 IEEE*, pages 1–6. IEEE, 2008.

[33] Yunwei Li, D Mahinda Vilathgamuwa, and Poh Chiang Loh. Design, analysis, and real-time testing of a controller for multibus microgrid system. *Power electronics, IEEE transactions on*, 19(5):1195–1204, 2004.

[34] Wan Quan Liu, M Paskota, Victor Sreeram, and KL Teo. Improvement on stability bounds for singularly perturbed systems via state feedback. *International journal of systems science*, 28(6):571–578, 1997.

[35] JA Peças Lopes, CL Moreira, and AG Madureira. Defining control strategies for microgrids islanded operation. *Power Systems, IEEE Transactions on*, 21(2):916–924, 2006.

[36] JA Peças Lopes, CL Moreira, and FO Resende. Control strategies for microgrids black start and islanded operation. *International Journal of Distributed Energy Resources*, 1(3):241–261, 2005.

[37] Ritwik Majumder, Balarko Chaudhuri, Arindam Ghosh, G Ledwich, and F Zare. Improvement of stability and load sharing in an autonomous microgrid using supplementary droop control loop. *Power Systems, IEEE Transactions on*, 25(2):796–808, 2010.

[38] Ritwik Majumder, Arindam Ghosh, Gerard Ledwich, and Firuz Zare. Angle droop versus frequency droop in a voltage source converter based autonomous microgrid. In *Power & Energy Society General Meeting, 2009. PES'09. IEEE*, pages 1–8. IEEE, 2009.

[39] Ritwik Majumder, Arindam Ghosh, Gerard Ledwich, and Firuz Zare. Load sharing and power quality enhanced operation of a distributed microgrid. *Renewable Power Generation, IET*, 3(2):109–119, 2009.

[40] Ritwik Majumder, Gerard Ledwich, Arindam Ghosh, Saikat Chakrabarti, and Firuz Zare. Droop control of converter-interfaced microsources in rural distributed generation. *Power Delivery, IEEE Transactions on*, 25(4):2768–2778, 2010.

[41] YARI Mohamed and Ehab F El-Saadany. Adaptive decentralized droop controller to preserve power sharing stability of paralleled inverters in distributed generation microgrids. *Power Electronics, IEEE Transactions on*, 23(6):2806–2816, 2008.

[42] P Moylan and D Hill. Stability criteria for large-scale systems. *Automatic Control, IEEE Transactions on*, 23(2):143–149, 1978.

[43] Paul Myles, Joe Miller, Steven Knudsen, and Tom Grabowski. 430.01. 03 electric power system asset optimization. *Morgantown, WV: National Energy Technology Laboratory*, 2011.

[44] Daniel E Olivares, Ali Mehrizi-Sani, Amir H Etemadi, Claudio A Cañizares, Reza Iravani, Mehrdad Kazerani, Amir H Hajimiragha, Oriol Gomis-Bellmunt, Maryam Saeedifard, Rodrigo Palma-Behnke, et al. Trends in microgrid control. *Smart Grid, IEEE Transactions on*, 5(4):1905–1919, 2014.

[45] M. A. Pai. *Energy Function Analysis for Power System Stability*. Springer, 1989.

[46] Paolo Piagi. *Microgrid control*. PhD thesis, University of Wisconsin–Madison, 2005.

[47] Paolo Piagi and Robert H Lasseter. Autonomous control of microgrids. In *Power Engineering Society General Meeting, 2006. IEEE*, pages 8–pp. IEEE, 2006.

[48] Amr Ahmed A Radwan and Yasser Abdel-Rady I Mohamed. Modeling, analysis, and stabilization of converter-fed ac microgrids with high penetration of converter-interfaced loads. *Smart Grid, IEEE Transactions on*, 3(3):1213–1225, 2012.

[49] Abdelhay A Sallam and Om P Malik. *Electric distribution systems*, volume 68. John Wiley & Sons, 2011.

[50] Nitish Saraf, Kenneth McIntyre, John Dumas, and Surya Santoso. The annual black start service selection analysis of ercot grid. *Power Systems, IEEE Transactions on*, 24(4):1867–1874, 2009.

[51] Peter W Sauer and MA Pai. *Power system dynamics and stability*, volume 4. Prentice Hall Upper Saddle River, NJ, 1998.

[52] Mahmoud A Sayed and Takaharu Takeshita. All nodes voltage regulation and line loss minimization in loop distribution systems using upfc. *Power Electronics, IEEE Transactions on*, 26(6):1694–1703, 2011.

[53] John W Simpson-Porco, Florian Dörfler, and Francesco Bullo. Droop-controlled inverters are kuramoto oscillators. In *IFAC Workshop on Distributed Estimation and Control in Networked Systems, Santa Barbara, CA, USA*, pages 264–269, 2012.

[54] John W Simpson-Porco, Florian Dorfler, and Francesco Bullo. Voltage stabilization in microgrids via quadratic droop control. In *Decision and Control (CDC), 2013 IEEE 52nd Annual Conference on*, pages 7582–7589. IEEE, 2013.

[55] Xisheng Tang, Wei Deng, and Zhiping Qi. Investigation of the dynamic stability of microgrid. *Power Systems, IEEE Transactions on*, 29(2):698–706, 2014.

[56] Jan C Willems. Dissipative dynamical systems part I: General theory. *Archive for rational mechanics and analysis*, 45(5):321–351, 1972.

[57] Jan C Willems. Dissipative dynamical systems part II: Linear systems with quadratic supply rates. *Archive for Rational Mechanics and Analysis*, 45(5):352–393, 1972.

[58] JL Willems and JC Willems. The application of lyapunov methods to the computation of transient stability regions for multimachine power systems. *Power Apparatus and Systems, IEEE Transactions on*, 89(5):795–801, 1970.

[59] HH Zeineldin, James L Kirtley Jr, et al. Microgrid stability characterization subsequent to fault-triggered islanding incidents. *Power Delivery, IEEE Transactions on*, 27(2):658–669, 2012.

[60] Yun Zhang and Le Xie. Online dynamic security assessment of microgrids interconnections for future smart distribution. *Power Systems, IEEE Transactions on*, 30(6):3246–3254, 2015.

[61] Yun Zhang and Le Xie. A transient stability assessment framework in power electronic-interfaced distribution systems. *Power Systems, IEEE Transactions on*, submitted, 2015.

[62] Yun Zhang, Le Xie, and Qifeng Ding. Interactive control of coupled microgrids for guaranteed system-wide small signal stability. *Smart Grid, IEEE Transactions on*, to appear, 2016.

[63] Jiebei Zhu, Campbell D Booth, Grain P Adam, Andrew J Roscoe, and Chris G Bright. Inertia emulation control strategy for vsc-hvdc transmission systems. *Power Systems, IEEE Transactions on*, 28(2):1277–1287, 2013.